CHAPTER 8

EVENT SELECTION

8.1 Analysis Strategy

This analysis aims to select events that would have small cross sections producing only a handful of events from the entire 139 fb^{-1}collected by ATLAS. The signature of two displaced leptons, is rather simple in principle, but this analysis had not been done before in the conditions of the LHC, so extensive optimization of the signal regions and lepton selection criteria needed to be done. A cut in the event selection should decrease or eliminate some background, but have little to no impact on the signal. For example, quality criteria ensure that leptons are well measured in the detector, and leptons from slepton decays will pass these quality criteria, but fake leptons from reconstruction failures generally will not. Every effort was made to remain as signal-agnostic as possible, so cuts on the specific topology of the GMSB SUSY decay were avoided.

This analysis is split into three signal regions, defined by the flavor of the two highest p_{T} leptons in the event: SR-ee with two electrons, SR-$\mu\mu$ with two muons, and SR-$e\mu$ with an electron and a muon. There are two definitions of leptons used: *baseline* and *signal*. Baseline leptons are required to pass the reconstruction and identification criteria described in subsection 5.3.2 and subsection 5.2.2 and have $p_{\text{T}} > 50$ GeV and $|d_0| > 2$ mm. Signal muons are required to further pass bespoke quality requirements, an isolation cut, and have $p_{\text{T}} > 65$ GeV and $|d_0| > 3$ mm. Displacement-independent quality variables, described in the rest of this chapter, were defined specifically for this analysis as many standard quality criteria place requirements on the $|d_0|$, $|z_0|$, or the number of hits in the Pixel detector, all of which would limit the ability to target displaced leptons.

8.1.1 Background Overview

The two signal leptons are required to have high p_{T} and high $|d_0|$, higher than that expected of any leptons resulting from SM processes. The remaining backgrounds come from failures of reconstruction algorithms, extreme tails of decays of Heavy Flavor (HF) physics (b-jets or τs), and muons from cosmic rays. None of these background sources are well modeled in MC, so data-driven methods must be used. This brings additional challenges from statistical limitations and care must be taken to avoid unblinding the signal regions.

Fake leptons result from the mis-association of a track to a calorimeter or MS signature, creating a reconstructed lepton that does not correspond to a real particle that passed through the detector. This is particularly likely due to use of LRT. The extended tracking algorithm loosens several requirements that enable high-$|d_0|$ tracking, but also introduces many *fake tracks*, combinations of hits that do not correspond to the trajectory of a particle in the detector. When matched to MS or calorimeter signatures, high-$|d_0|$ leptons can be created and form a background to this search. This is particularly likely to occur during electron reconstruction, where the track can be associated to real calorimeter signatures from photons or converted photons.

The background to SR-$\mu\mu$ is dominated by cosmic ray muons. The ATLAS detector is far underground partially to avoid the many particles from cosmic rays passing through the detector. However, there is a service shaft above the detector and muons can make it through the earth above the detector, so muons from cosmic rays are constantly passing through the detector. If a muon from a cosmic ray passes through the detector and is coincident with a bunch crossing, the event could be triggered and that muon reconstructed. Since it can pass at any point with respect to the collision, it can be reconstructed as one or two muons with high $|d_0|$, exactly mimicking the targeted signature.

Both electrons and muons suffer potential backgrounds from HF decays, predominately from the decays of b-hadrons. b-quarks are very commonly produced in LHC collisions and they immediately hadronize into b-hadrons, which have a lifetime of 1.5 ps and whose decays

include a lepton 11% of the time [9]. This is sufficiently long that the b-hadron travels far enough before it decays such that a secondary vertex can be identified. Generally, the tracks have low p_{T} and maximum $|d_0|$ of about 1.5 mm, and the 3 mm cut on signal leptons is designed to minimize this effect. However, it is possible that extreme tails of this distribution are not well modeled in MC and in an analysis where 0 background events are expected, understanding each possible source is paramount.

8.2 Event Requirements

Events must pass a trigger in order to be recorded by the ATLAS detector. Three different triggers are used in this analysis and the data separated into three orthogonal regions based on the topology of the event, described in Table 6.1. The trigger is required to pass in the appropriate region for the event to be selected.

Each event is required to pass a standard set of ATLAS event quality preselection criteria. Specifically, these include detector error flags which reject events with noise bursts or data corruption, or events in periods where any sub-detector was operating suboptimally. Events are required to have at least one PV with $|z| < 200$ mm.

From events that pass the previous two requirements, events are sorted into the three signal regions based on the highest p_{T} baseline leptons in the event. Leptons in signal events are required to be well separated with $\Delta R_{\ell\ell} > 0.2$. This eliminates background from lepton pairs that could be created from an interaction with the material of the detector. Finally, signal events are required to have zero cosmic muons. The cosmic tag and the associated background will be discussed in subsection 9.3.1. The analysis was optimized and the backgrounds estimated while keeping the SRs blinded, so Control Regions (CRs) (where backgrounds are estimated) and Validation Regions (VRs) (where additional studies and validation are done) are defined with different numbers of leptons and cosmic tags. All CRs and VRs are designed to be dominated by backgrounds and have very few signal events in them. A full list of all signal, control, and validation regions can be seen in Table 8.1.

8.3 Electrons

Quality cuts specifically designed for this analysis are introduced to eliminate fake electrons reconstructed from the incorrect association of tracks and calorimeter clusters. The most important of these cuts is

$$\Delta p_{\mathrm{T}}/p_{\mathrm{T}} \equiv \frac{p_{T,\mathrm{track}} - p_{T,e}}{p_{T,e}} \tag{8.1}$$

which measures the degree of consistency between the p_{T} of the electron, which is dominated by the calorimeter measurement, and the p_{T} of the track. Fake tracks tend to be low p_{T}, resulting in fake electrons with tracks with less than half of the p_{T} of the electron, $\Delta p_{\mathrm{T}}/p_{\mathrm{T}} < -0.5$,.

Additionally, quality requirements are imposed on the ID tracks. They are required to have $\chi^2_{\mathrm{ID}} < 2$ [1] and no more than 1 missing hit after the first hit in the track. These cuts remove poor hit combinations, short tracks, or tracks missing measurements. Additionally, signal electrons are required to be isolated and pass the `FCTight` isolation definition described in section 5.5

8.4 Muons

Signal muon requirements are similar to those placed on signal electrons. The muon is required to have $\chi^2_{\mathrm{CB}} < 3$ in order to ensure a good combination between ID track and MS track, similar to the $\Delta p_{\mathrm{T}}/p_{\mathrm{T}}$ cut on electrons. Additionally, signal muons are required to pass the same ID track quality requirements as electrons as well as MS track quality requirements. Requiring $N_{\mathrm{prec}} \geq 3$ (number of MDT layers with at least 3 hits) and $N_{\phi} \geq 1$ (number of RPC hits) ensure that the MS track is well measured in both its η and ϕ coordinates. Signal muons required to pass the `FCTight` isolation requirement described in section 5.5.

Furthermore, muons are required to have $t_0^{\mathrm{avg}} < 30$. t_0^{avg} is the average t_0 calculated from the MS segments associated to the muon. The measurement of t_0 is described in

1. In this thesis, χ^2 implies χ^2 divided by the number of degrees of freedom in the fit

section 4.4.1. If the fit fails, the segment is assigned $t_0 = 0$, and this value does not enter the t_0^{avg} calculation, but muons that have all segments with $t_0 = 0$ are not rejected. This cut is designed to better control the background from cosmic muons, which have a much wider spread in t_0^{avg} than collision muons.

8.5 Acceptance and Efficiency

Acceptance is defined as the fraction of events that could enter the SR based on their kinematics, and efficiency is fraction of the accepted events that get correctly identified. The acceptance and efficiency in this analysis are both rather low. The exponential nature of the p_{T} and $|d_0|$ distributions of the $\tilde{\ell}$ decays, many daughter leptons have low p_{T} and low $|d_0|$ and do not pass the signal kinematic selections and are not accepted. This particularly effects low mass, low lifetime $\tilde{\ell}$; the p_{T} cut has an even stronger impact on leptons from $\tilde{\tau}$ decays, which must decay through a standard model τ. Conversely, the degradation of the LRT efficiency at high $|d_0|$ means that leptons with high $|d_0|$ are often not reconstructed. This particularly effects $\tilde{\ell}$ with long lifetimes. Additionally, the p_{T} and $|d_0|$ and η cuts required to pass one of the triggers used in this analysis to pass the LRT filters further reduces the acceptance and efficiency.

The acceptance is highest for lifetimes around 0.1 ns, around 30% for $\tilde{\mu}$ and $\tilde{e}$ production and only 0.5% or $\tilde{\tau}$ production. The efficiency is higher, around 50% for lifetimes of order 0.1 ns for all flavors of $\tilde{\ell}$. The values for a range of possible mass and lifetime points can be see in Figure 8.1, Figure 8.2, Figure 8.3

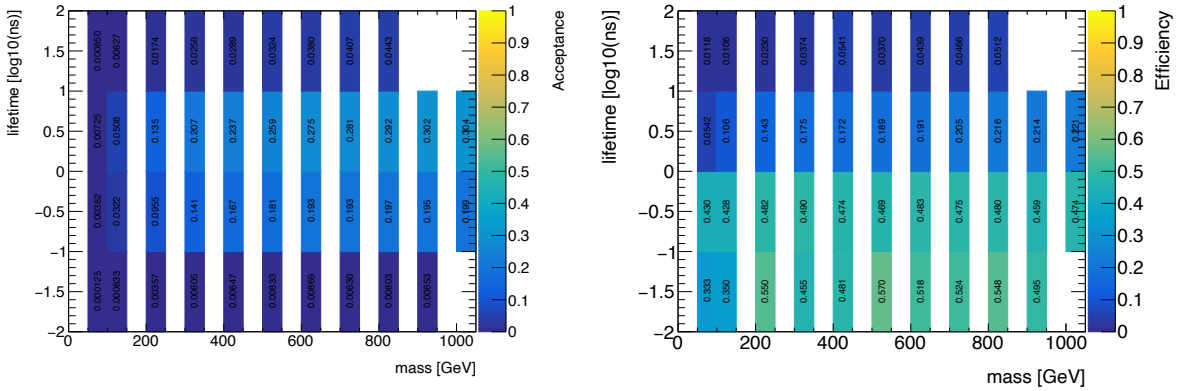

Figure 8.1: Acceptance (left) and efficiency for $\tilde{\mu}$ decaying to muons in SR-$\mu\mu$. The x-axis shows the possible masses of the $\tilde{\mu}$ and the y-axis its possible lifetime.

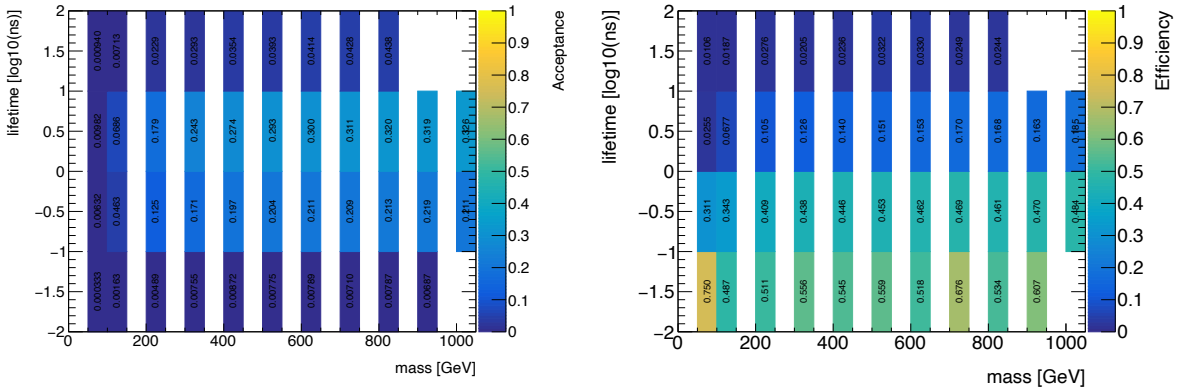

Figure 8.2: Acceptance (left) and efficiency for $\tilde{e}$ decaying to electrons in SR-ee. The x-axis shows the possible masses of the $\tilde{e}$ and the y-axis its possible lifetime.

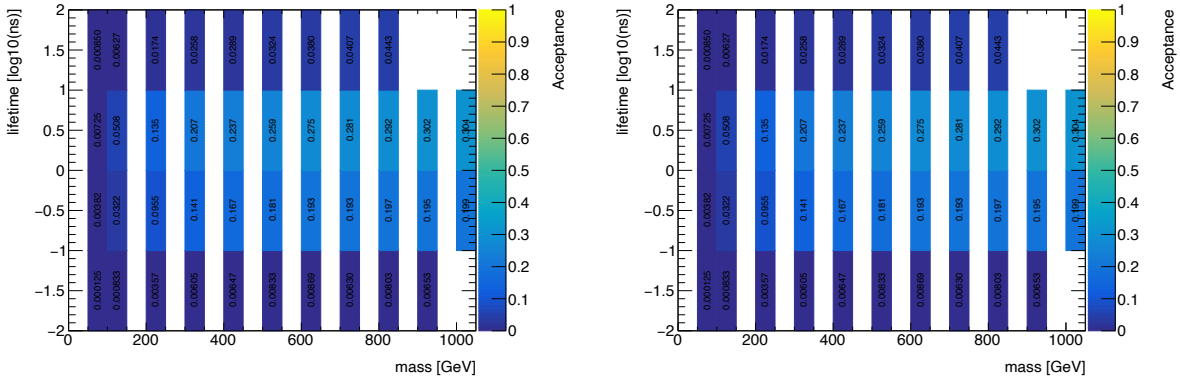

Figure 8.3: Acceptance (left) and efficiency for $\tilde{\tau}$ s decaying to taus in SR-$\mu\mu$, SR-ee, and SR-$e\mu$ combined. The x-axis shows the possible masses of the stau and the y-axis its possible lifetime.

Purpose	Name	# of Leptons	# of Cos.Tags	Additional Requirements
Signal Regions	SR-ee	≥ 2 e	0	
	SR-$\mu\mu$	≥ 2 μ	0	
	SR-$e\mu$	≥ 1 e, ≥ 1 μ	0	
Control Regions				
Fake Estimation	CR-ee-fake	≥ 2 e	0	≥ 2 loosened electrons, not in SR-ee
	CR-$e\mu$-fake	≥ 1 e, ≥ 1 μ	0	≥ 2 loosened leptons, not in SR-$e\mu$
Heavy Flavor Estimation	CR-$\mu\mu$-hf	≥ 2 μ	0	≥ 1 anti-isolated ℓ, loosened p_{T} and d_0
Cosmic Estimation	CR-M_{full}	$\geq 1\mu$	≥ 1	includes muons failing N_ϕ and N_{prec} cuts
	CR-$\mu\mu$-topbad	≥ 2 μ	0	one signal and one loosened muon
Validation Regions				
Cut Evaluation	VR-M_{narrow}	$\geq 1\mu$	≥ 1	using narrow cosmic tag
	VR-e	1 e, 0 μ	0	electron is baseline
	VR-μ	0 e, 1 μ	0	muon is baseline
Fake Validation	VR-ee-fake	≥ 2 e	0	inverted $\Delta p_{\mathrm{T}}/p_{\mathrm{T}}$ selection
	VR-ee-fake-hf	≥ 2 e	0	≥ 1 anti-isolated ℓ, loosened quality
	VR-$e\mu$-fake	≥ 1 e, ≥ 1 μ	0	1 e fails $\Delta p_{\mathrm{T}}/p_{\mathrm{T}}$, 1 μ fails χ^2_{CB}
	VR-$e\mu$-fake-hf	≥ 1 e, ≥ 1 μ	0	1 e fails $\Delta p_{\mathrm{T}}/p_{\mathrm{T}}$, no isolation req., loosened quality
Cosmic Validation	VR-μM_{full}	≥ 2 μ	1	
	VR-μ-narrow	≥ 1 μ	0*	using narrow cosmic tag
	VR-μM_{narrow}	≥ 2 μ	1*	using narrow cosmic tag

Table 8.1: Summary of signal, control and validation regions used in the analysis. All regions are defined exclusively by their reconstructed leptons. In the table, all leptons should be assumed to be signal leptons except for their noted deviation from the signal requirements. All requirements are placed on the two leading leptons, additional leptons are allowed in the event but no selections are made on them. In each region, the appropriate trigger selection is made. In region names, a capital M denotes a cosmic-tagged muon, and for requirements on numbers of cosmics, all leptons in the event are considered. An * on the number of cosmic tags denotes the number of muons tagged or untagged by the narrow tag, not the nominal tag used in the signal regions.

Electron Selections	
p_{T}	> 65 GeV
$\lvert d_0 \rvert$	> 3 mm
$\lvert \eta \rvert$	< 2.47
Isolation	`FCTight`
$\Delta p_{\mathrm{T}}/p_{\mathrm{T}}$	$\geq$ -0.5
χ^2_{ID}	< 2
N_{miss}	≤ 1

Table 8.2: Overview of electron signal selections.

Muon Selections	
p_{T}	> 65 GeV
$\lvert d_0 \rvert$	> 3 mm
$\lvert \eta \rvert$	< 2.5
Isolation	`FCTight`
N_{prec}	≥ 3
χ^2_{CB}	< 3
N_ϕ	≥ 1
χ^2_{ID}	< 2
N_{miss}	≤ 1
$\lvert t_0^{\mathrm{avg}} \rvert$	< 30
Pass Cosmic Veto	True

Table 8.3: Overview of muon signal selections.

CHAPTER 9

BACKGROUNDS

In this analysis, backgrounds are estimated per signal region. In SR-ee and SR-$e\mu$, algorithmic fakes are the dominant source of background. In SR-$\mu\mu$, the background contribution from algorithmic fake muons and muons from heavy flavor decays is negligible ($\mathcal{O}(10^{-4})$), and the dominant background is from cosmic muons coincident with LHC collisions. While the signal lepton selection and event selection described in the previous chapter very efficiently remove these backgrounds, background estimates are calculated to estimate any residual contribution. All backgrounds are not well modeled in MC, so must be estimated from CRs in data, often resulting in statistical limitations.

9.1 Background to SR-ee

9.1.1 Fakes and Heavy Flavor Decays

The primary background to SR-ee is algorithmic fakes from the misassociation of a track with a real energy deposit in the EM calorimeter (such as from a photon); there is a secondary contribution from electrons from HF decays. MC samples of $t\bar{t}$ along with a photon dominated sample (described in section 6.2) were used to study the relative contributions.

The $t\bar{t}$ provides a sample of HF decays (though not the dominant source of HF decays at the LHC), yet after all of the signal requirements, the remaining high $|d_0|$ electron was the result of a photon combined with an ID track. That this sample has many more b-hadron decays than photons, yet the photons contribute a larger background even in this narrow region of phase space, indicates that algorithmic fakes are the larger contributer of background events to SR-ee. Additionally, in truth-level studies of background MC, such as $BB \to \mu\mu$ (at truth level, the electron and muon kinematics are the same), $Z \to \tau\tau$ (where the τ decays include electrons), and $t\bar{t}$, all show exponentially falling distributions with no two lepton events that pass the p_{T} and $|d_0|$ cuts in the SR, as designed.

Further studies were performed in data, with one baseline electron passing the filter requirements and another lepton with no $|d_0|$ cut made. This second lepton must be *anti-isolated*, meaning it fails the isolation requirement made on signal leptons and has substantial activity surrounding it in the calorimeter and/or the ID and is likely to be inside of a jet. While the $\Delta p_{\mathrm{T}}/p_{\mathrm{T}}$ cut is designed to remove algorithmic fakes, it is a very effective remover of anti-isolated electrons as well. Clusters associated to electrons reconstructed inside of jets are likely to have additional energy incorrectly added to their clusters, increasing the cluster p_{T} and decreasing the $\Delta p_{\mathrm{T}}/p_{\mathrm{T}}$. Thus, it is not possible to disentangle heavy flavor electrons from fake electrons and the background contributions are estimated together with fakes as the dominant contribution.

9.1.2 Background Estimate

Fake electrons result from the failure of the reconstruction algorithm algorithm, and so the two fake electrons in an event should be uncorrelated. This assumption is used to estimate the background with an *ABCD method*. The procedure divides events into four regions based on the quality of the leading and subleading leptons in the event, shown in Figure 9.1. The number of events in regions B, C, and D are combined to estimate the number of events in region A, the signal region:

$$N_A = \frac{N_B}{N_D} \times N_C \tag{9.1}$$

In the nominal estimate, region A is the signal region, with two electrons passing all signal cuts, region D has both electrons failing at least one signal cut, and regions C and D have only one electron passing all signal cuts while the other fails at least one (regions B, C, and D compose CR-*ee*-fake). For this estimate, a "failing" electron fails one of the $\Delta p_{\mathrm{T}}/p_{\mathrm{T}}$, χ^2_{ID}, or N_{miss} requirements, while a "passing" electron is a signal electron, passing all three cuts. The number of events in each region and the estimated number of events in SR-*ee* is

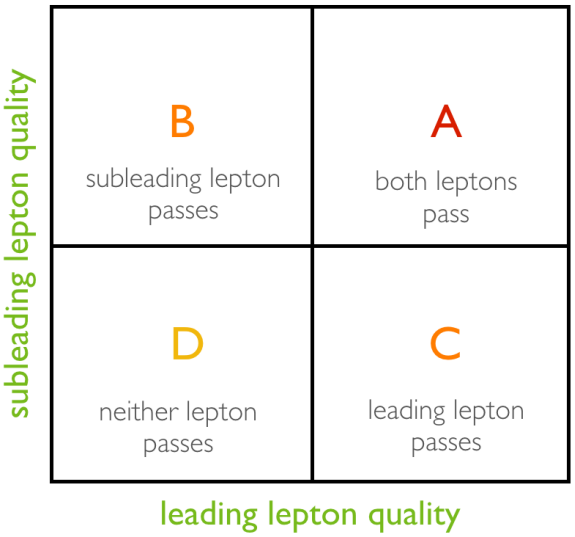

Figure 9.1: The regions used for ABCD estimation.

shown in Table 9.1.

9.1.3 Validation and Systematic Uncertainties

The definitions of the ABCD regions can be varied to perform validations of the estimate and quantify systematic uncertainties. There are two ways to do this: first, the estimate can be done in slightly different ways, and the difference from the nominal estimate taken as an uncertainity; second, an estimate can be done in a validation region, where one or more signal cuts are inverted, and the estimated number of events can be compared to the actual number of events in region A. In the second scenario, one looks for *closure*, that the estimate correctly estimates the number of events (within statistical uncertainties), giving evidence that the method and its assumption are sound. If this is not the case, the *nonclosure*, the extent to which the estimate disagrees with the correct number of events, is evaluated and an uncertainty can be taken to cover this.

Validations are performed by estimating the number of events in SR-*ee* in different ways. For example, only the $\Delta p_{\mathrm{T}}/p_{\mathrm{T}}$, the most effective fake discriminator, is used as the "pass-

Region	Nominal	Only $\Delta p_{\mathrm{T}}/p_{\mathrm{T}}$
D Observed	9068	1440
C Observed	77	28
B Observed	54	19
A Estimate	0.459 ± 0.082	0.37 ± 0.11

Table 9.1: Results of the ABCD estimate for the nominal SR-*ee* estimate, the number of events in each region are shown as well as the estimate for A. The uncertainties are statistical only and using Poisson statistics.

ing"/"failing" variable. The results of this estimate are also shown in Table 9.1, the results are consistent within statistical uncertainties but the nominal estimate is more precise.

The second kind of validation is performed in two regions: one that enhances the fake contribution, and a second that enhances the HF contribution. First, in a fake enhanced region, VR-*ee*-fake, where the $\Delta p_{\mathrm{T}}/p_{\mathrm{T}}$ cut is inverted and the estimate is performed with χ^2_{ID} and N_{miss} together as the "passing"/"failing" variables. This changes the estimate to predicting the number of fake electrons (failing $\Delta p_{\mathrm{T}}/p_{\mathrm{T}}$) from regions with electrons that are more fake (failing $\Delta p_{\mathrm{T}}/p_{\mathrm{T}}$ and one or both of χ^2_{ID} and N_{miss}). In this region, 1440 events are observed, and 1356 $\pm$ 49 are predicted. Even though this result is consistent within the statistical uncertainties, the difference between the central values (6.2%) is taken as a nonclosure and applied as a systematic uncertainty on the SR estimate.

Next, a validation is done in a HF enhanced region, VR-*ee*-fake-hf, which is identical to CR-*ee*-fake with the additional requirement that at least one electron is anti-isolated. This additional requirement reduces the statistics in the region quite a bit, so the electron cuts are loosened to $p_{\mathrm{T}} > 50$ GeV, $|d_0| > 2$ mm, and instead of the usual $\Delta p_{\mathrm{T}}/p_{\mathrm{T}}$ cut at -0.5, they must satisfy $\Delta p_{\mathrm{T}}/p_{\mathrm{T}} > -0.9$. Electrons in dense environments are more likely to have extra energy added to their clusters or have the wrong track associated, so the $\Delta p_{\mathrm{T}}/p_{\mathrm{T}}$ cut must be loosened to probe the subdominant HF contribution to the SR-*ee* background. In this region, 23.5 ± 1.9 events were predicted, and 26 were seen. Again, the results are consistent within uncertainties, with only a 11% difference in central values. This difference is taken as a systematic uncertainty.

9.1.4 Summary

This estimate is dominated by statistical uncertainties with additional, conservative, systematic uncertainties taken, giving a final estimate of 0.46 ± 0.10 (0.082 stat. and 0.058 syst). This estimate has the smallest uncertainty of the three SRs due to the sufficient statistics in the estimate regions.

9.2 Background to SR-$e\mu$

9.2.1 Fake Background

The background to SR-$e\mu$ is very similar to the background in SR-ee and is estimated in a similar way. By tagging a lepton that fails either isolation or quality requirements and studying the properties of the other, probe lepton, the main contributing background (either fake or HF) is determined. Of the probe leptons, 100 pairs failed some signal requirements, but none only failed isolation, indicating that as in the case of SR-ee, algorithmic fakes are the dominant background to SR-$e\mu$.

Fake muons are rare compared to fake electrons due to the lack of extraneous activity in the MS compared to the calorimeter where photons add ambiguity to electron reconstruction. As a result, this estimate is extremely statistically limited.

9.2.2 Background Estimate

As in SR-ee, the two fake leptons in the event should be uncorrelated and so an ABCD method is used to estimate the background. A "failing" electron (as in SR-ee) is one that fails any one of the $\Delta p_{\mathrm{T}}/p_{\mathrm{T}}$, χ^2_{ID}, or N_{miss} requirements, a "failing" muon fails any one of the χ^2_{ID}, χ^2_{CB}, N_{miss}, N_{prec}, or N_{ϕ} requirements, and in both cases "passing" indicates a signal electron or muon.

However, when performing this estimate, the B region (electron passes, muon fails) has only 1 event, and the C region (muon passes, electron fails) has 0 events. This result cannot

be used to calculate a background estimate, but it can be used to place an upper bound by setting the number of events in the C region to 1 event. The total number of events in SR-$e\mu$ must be less than 0.012 ± 0.017, where the uncertainty is statistical only. In order to increase the statistical power, different combinations of "passing" and "failing" leptons were required to only pass the baseline kinematic cuts of $p_{\mathrm{T}} > 50$ GeV and $|d_0| > 2$ mm. Allowing both passing and failing leptons to only meet the baseline requirements allowed 1 event in the C region, enabling a background estimate of $0.007^{+0.018}_{-0.009}$. Statistical uncertainties are quoted using the Wilson interval for the C/D ratio summed in quadrature with the Poisson uncertainty on the number of events in the B region. This is taken as the nominal upper bound and the full result of this loosening can be seen in Table 9.2.

Estimate Region	signal p_{T}, $\lvert d_0\rvert$ cuts on all ℓ	signal p_{T}, $\lvert d_0\rvert$ cuts on passing ℓ	no signal p_{T}, $\lvert d_0\rvert$ cuts
D Observed	81	139	138
C Observed	0	0	1
B Observed	1	1	1
A Estimate	$< 0.012 \pm 0.017$	$< 0.007 \pm 0.010$	$0.007^{+0.018}_{-0.009}$

Table 9.2: Results of the ABCD method in the $e\mu$ channel in which the d_0 and p_{T} requirements are selectively loosened from 65 to 50 GeV, and 3 to 2 mm. The first column shows the results without any loosening, the second shows the results with the loosening applied only to the failing leptons, and the final column shows the results with the loosening applied in all regions. Uncertainties are statistical only. For the upper bound results, the value is obtained by setting the C region to 1 event, and the uncertainties are calculated using Poisson statistics. In the final case, the full calculation can be done.

9.2.3 Validation and Systematic Uncertainties

As in the case of SR-ee, validations are performed enhancing the fake or HF contributions. VR-$e\mu$-fake again inverts the most powerful fake discriminators, $\Delta p_{\mathrm{T}}/p_{\mathrm{T}}$ for electrons and χ^2_{CB} for muons with the loosened p_{T} and $|d_0|$ cuts. In this region, 2 events are observed in the A region compared to $1.9^{+1.8}_{-1.0}$. While these agree within the very large uncertainties, a 7.8% nonclosure systematic uncertainty is taken from the difference in central values.

Then, VR-$e\mu$-fake-hf is defined requiring at least one anti-isolated lepton with loosened

p_{T} and $|d_0|$ cuts. To increase statistics, the $\Delta p_{\mathrm{T}}/p_{\mathrm{T}}$ cut is again loosened to -0.9 and the cuts on N_{prec} and N_{ϕ} are removed. Here, one event is observed in the A region, and $0.38^{+0.37}_{-0.32}$ events are predicted. To attempt this estimate another way with more statistical power, the estimate is performed again in this region, this time remaining agnostic to whether or not the lepton is isolated. This results in an estimate of $2.6^{+2.0}_{-1.4}$, while 5 events are observed. These numbers are again consistent within their substantial statistical uncertainties, but a conservative 92% nonclosure uncertainty is taken to account for the difference between the central values.

9.2.4 Summary

This region is extremely statistically limited such that a full background estimate is not possible, and so an upper limit is set. Less than $0.007^{+0.019}_{-0.011}$ ($^{+0.018}_{-0.009}$ syst. and 0.006 stat.) background events are expected in SR-$e\mu$.

9.3 Background to SR-$\mu\mu$

9.3.1 Cosmic Muon Identification

Muons from cosmic rays constantly pass through the earth and thus the ATLAS detector, particularly through the service shaft above the detector where there is no layer of earth above the detector[1]. If a cosmic ray muon were coincident with a bunch crossing, the event could be triggered, reconstructed, and enter the dataset used for this analysis. The cosmic ray muon could pass through the entire detector at any distance from the PV, interacting with the ID and MS, and be reconstructed as two muons with high $|d_0|$, passing all quality variables (because the signature comes from a real muon) exactly mimicking the signature

1. The cosmic muon flux at sea level is about 1 μ per cm^2 per minute at sea level. ATLAS is approximately 46 m long and 50 m wide and a single data-taking run lasts 8 hours. That's 10^{10} cosmic muons per run! Of course, most of ATLAS is more than 50 m underground, which absorbs most of the cosmic muons. A muon from a cosmic ray must also be exactly coincident with a bunch crossing to be triggered and well reconstructed. *[TODO: Do this better with the flux under ground]*

of SR-$\mu\mu$.

A very efficient cosmic tag was defined for this analysis to identify and remove muons from cosmic rays. This is done using a reoptimization of the strategy used by Ref .[33]. This method first defines a spatial cosmic identification, and then conservatively tags all muons which would be impossible to identify using this method due to gaps in detector coverage. The cosmic muon, $\mu_{\rm cos}$, passes through the entire detector and gets reconstructed as two muons, one on the top of the detector ($\phi > 0$) referred to as $\mu_{\rm t}$ and the other on the bottom ($\phi < 0$), called $\mu_{\rm b}$. They follow the relationships

$$\Delta\phi = |\phi_{\mu_t} - \phi_{\mu_b}| = \pi \tag{9.2}$$

and

$$\Sigma\eta = |\eta_{\mu_t} + \eta_{\mu_b}| = 0 \tag{9.3}$$

The combination of these variables form a useful variable to describe events with 2 cosmic muons.

$$\Delta R_{\rm cos} = \sqrt{((\phi_{\mu_t} - \phi_{\mu_b}) - \pi)^2 + (\eta_{\mu_t} + \eta_{\mu_b})^2} \tag{9.4}$$

and it is useful to define

$$\Delta\phi_{cos} \equiv (\phi_0 - \phi_1) - \pi \tag{9.5}$$

and

The muon reconstruction algorithm described in section 5.2 uses the momentum direction measured in the MS in its extrapolation from MS track to ID track and . In 90% of cases only $\mu_{\rm b}$ is reconstructed and identified, while the detector signature for $\mu_{\rm t}$ exists but the fully reconstructed muon does not. Thus it is advantageous to tag a cosmic muon as one which is back to back with activity in the MS, not as two muons back to back, illustrated in Figure 9.2. A cosmic veto is defined based on the $\Delta\phi_{\rm cos}$ and $\Sigma\eta$ between a muon and a MS segment.

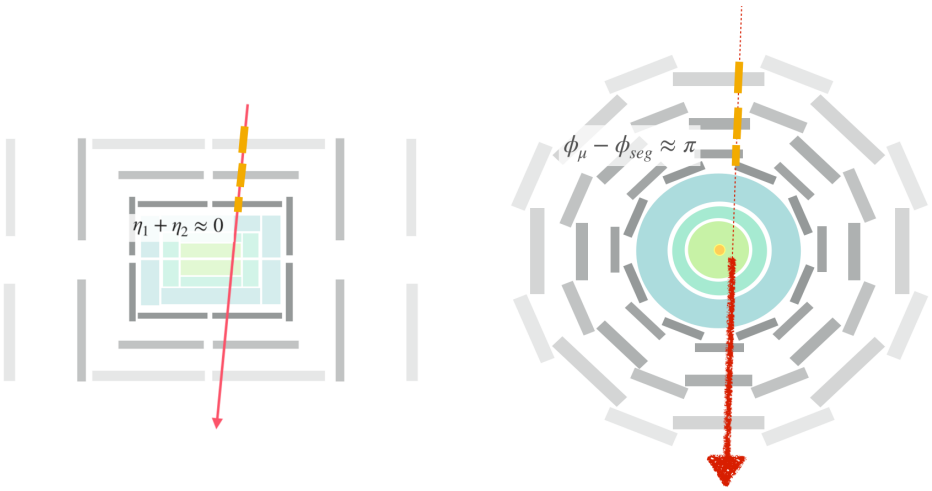

Figure 9.2: A sketch of a cosmic passing through the ATLAS detector, illustrating why the tag is designed the way that it is. This image is slightly adapted from Ref. [**ATLAS-CONF-2019-006**]

Since the MS is so far from the PV, the z_0 of individual MS segments is not measured and they are defined to point back to the origin. This creates a mismatch between the η of the segment and the η of the reconstructed muon in the determination of the cosmic tag. This is geometrically corrected for by re-calculating the $\Delta\eta$ between the segment and the muon in the cosmic veto calculation. A schematic of this correction is shown in Figure 9.3, its effect on the η and $\Sigma\eta$ measurements of muons in data is shown in Figure 9.4, and its effect on the $\Delta\phi_{\text{cos}}$-$\Sigma\eta$ distribution of cosmic and signal muons shown in Figure 9.5. This narrows the distribution of cosmic muons by an order of magnitude in $\Sigma\eta$. This distribution is isotropic for signal muons, so this definition allows for high cosmic muon rejection with minimal signal rejection.

The distribution the $\Delta\phi_{\text{cos}} - \Sigma\eta$ distribution is much narrower in $\Sigma\eta$ than in $\Delta\phi_{\text{cos}}$. This is because the MS measures η with an extremely high precision in the MDTs ($\mathcal{O}(10\ \mu\text{m})$), since it is the bending direction of the toroid and thus gives the momentum measurement, while the ϕ is measured by the RPCs with an order of magnitude less precision ($\mathcal{O}(10\ \text{mm})$). A high precision ϕ measurement of the combined muon comes from the ID, but the cosmic tag must contend with these resolution limitations to find a muon segment.

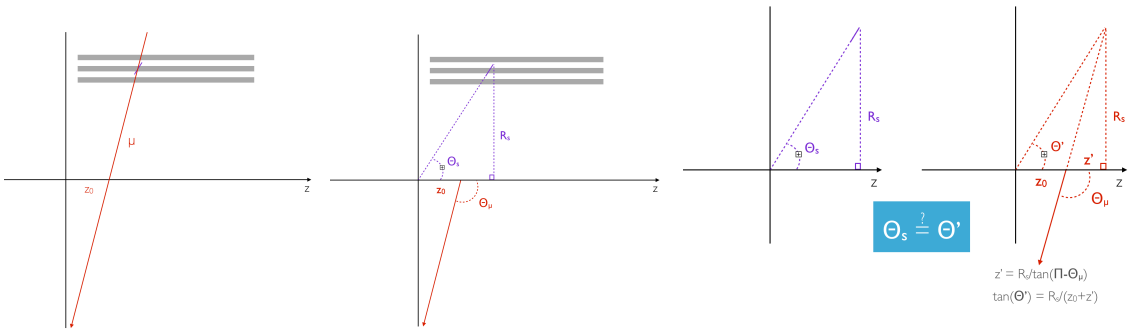

Figure 9.3: This series of figures shows the problem of the η recalculation. The MS segment should be measured as back to back in η and ϕ with the muon, because it is really one high p_T object moving through the whole detector. However, because the MS segments are reconstructed assuming they come from the origin, they will not actually be measured as back-to-back with the muon. The η that would be measured by a segment back to back with the muon is calculated, and compared to the η of all other segments in the event.

Tag	$\Delta\phi$(muon, segment)	$\Sigma\eta$(muon, segment)	Pass Coverage Acceptance	Rejection Efficiency
Full	< 0.25	< 0.018	True	99.5%
Narrow	< 0.02	< 0.013	True	59%

Table 9.3: Cuts applied in full and narrow cosmic tags. The narrow is contained in the full tag. An intermediate tag is defined as the region between the full and narrow tags, that is, tagged by the full but not the narrow tag.

Additionally, there are gaps in the MS to allow for detector access, so a muon is conservatively tagged as a cosmic if it is back to back with this gap in detector coverage, as it could not be tagged as a cosmic using the geometric algorithm. A map of the material of the MS is used to veto cosmic muons using this *detector coverage veto*. Figure 9.6 shows the impact of each step on the muon distribution in VR-μ, which is dominated by muons from cosmic rays.

For this analysis, two different definitions of a "cosmic muon" are used. The *nominal tag* is used to veto events in the SR. If any baseline muon is tagged by the nominal cosmic tag, the entire event is vetoed. A second *narrow tag* is used during the validation of the estimate of background from cosmic muons. Both tags require muons to pass the detector coverage veto. Table 9.3 describes the values used for the various cosmic tags used and Figure 9.7 shows the cuts used in the $\Delta\phi_{\cos}$-$\Sigma\eta$ distribution.

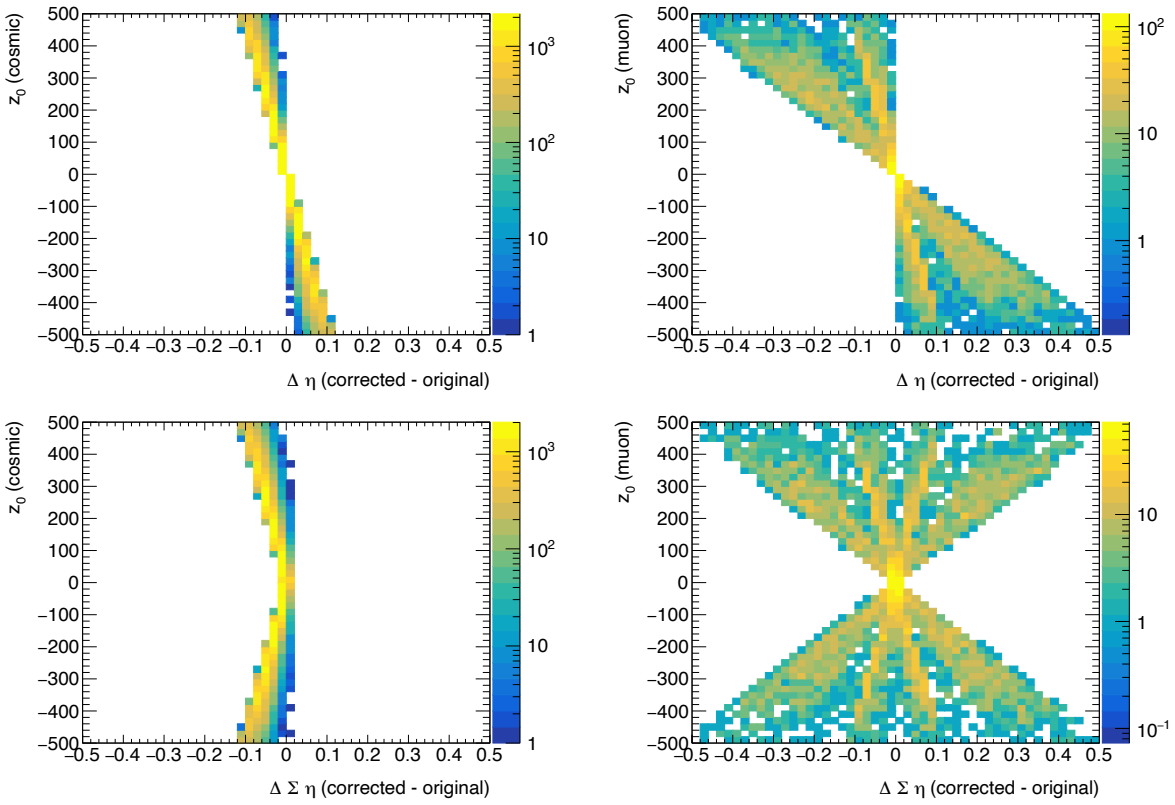

Figure 9.4: Change to the η measurement (top) and $\Sigma\eta$ measurement (bottom) due to the z_0 correction. These plots compare muons tagged with due to the presences of a segment in the $\Delta\phi_{\cos}$-$\Sigma\eta$ window (left) to those untagged or tagged with the detector coverage veto (right). The behavior shows isotropic effect for the muons which are not tagged via the algorithm that uses this correction, while the $\Sigma\eta$ distribution of cosmic muon always decreases due to the correction.

The cosmic tagging efficiency is determined by fitting distributions in VR-μ. A template of the t_0^{avg} of cosmic tagged muons and prompt (collision) muons is taken from data shown on the left of Figure 9.8. Any correlation between t_0^{avg} and d_0 can not be observed within detector resolutions, so the prompt sample of muons is taken to represent the signal muons that would result from collisions.

These are used to determine the fraction of cosmic muons in VR-μ before and after the cosmic tagged muons are removed from VR-μ (left of Figure 9.8). From the fraction of cosmic muons estimated from the template fitting, the fraction of muons removed by the cosmic tag can be measured. The nominal tag removes 99.5% of cosmic muons and the

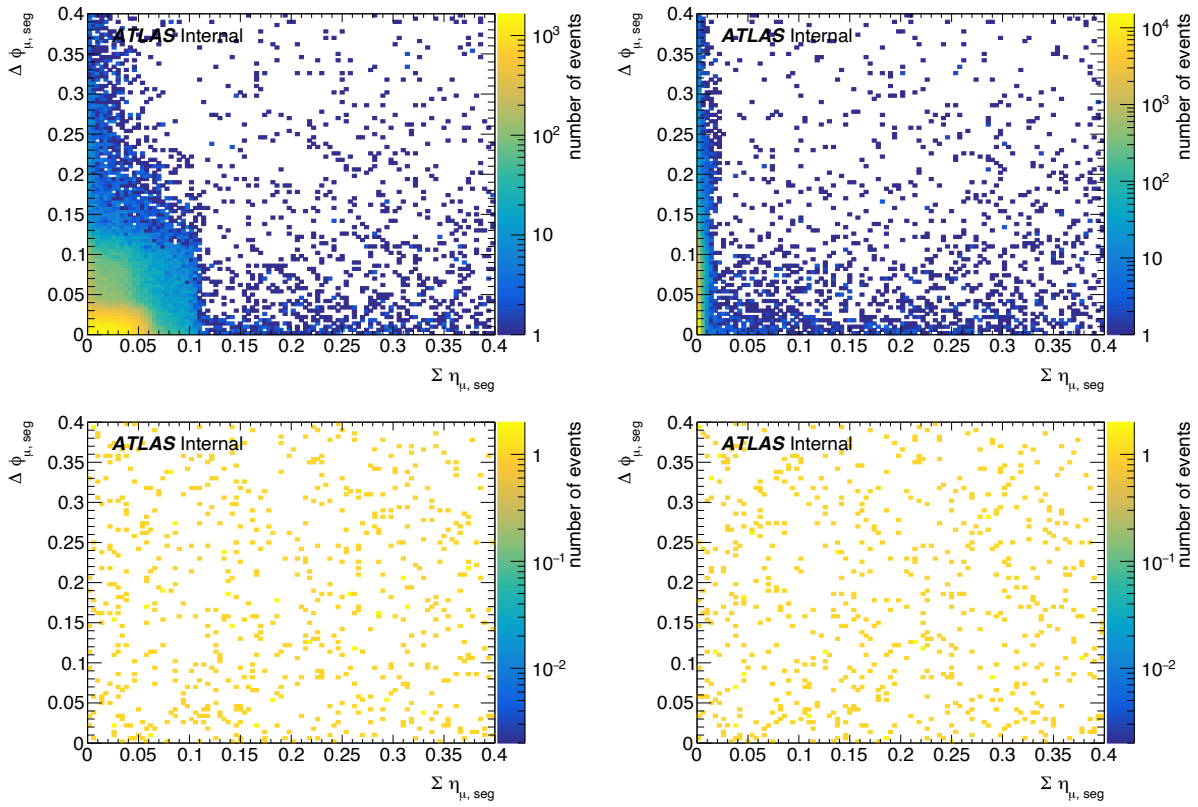

Figure 9.5: The $\Sigma\eta - \Delta\phi$ distribution is shown before (left) and after (right) the η recalculation. The top row shows the distributions in VR-μ and bottom row 300 GeV $\tilde{\ell}$ signal samples in our full range of lifetimes. Using this cosmic tag, a very tight cut can be made on cosmic muons without losing signal efficiency.

narrow tag removes 59% of cosmic muons. The nominal tag removes 8% of collision muons, primarily from the detector coverage veto. Figure 9.9 compares the kinematic distributions and cosmic-tagging efficiency between VR-μ and signal MC.

9.3.2 Properties of Events with Cosmic Tagged Muons

Because all all events with a cosmic tagged muon are vetoed, a CR with at least one cosmic tagged muon, CR-M_{full}, is defined to study cosmic events. 90% of events in CR-M_{full} have only one muon, and that muon is cosmic tagged. 90% of those events find the cosmic muon on the bottom of the detector, μ_{b}. The other 10% of events have two reconstructed muons and they are both cosmic tagged. One event was seen that had four cosmic tagged muons,

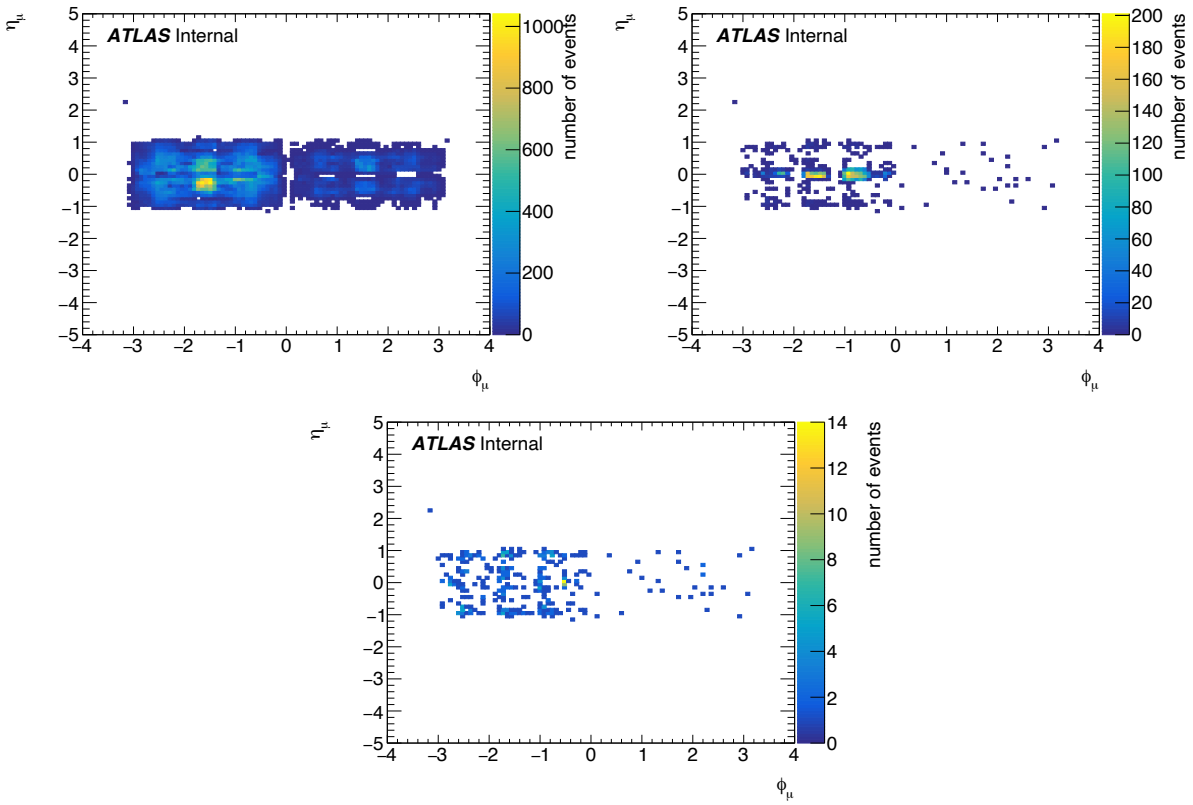

Figure 9.6: The $\eta - \phi$ distribution of muons in VR-μ are shown after baseline cuts (top left), the cosmic veto (top right), then the detector coverage veto (bottom).

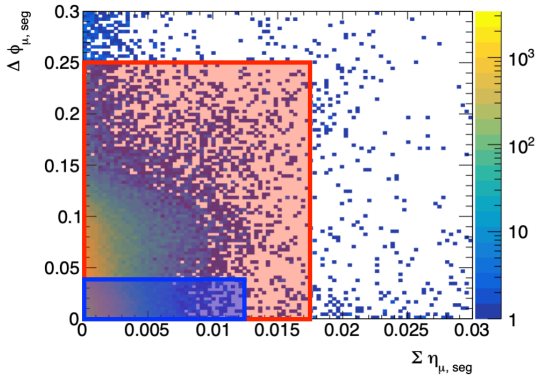

Figure 9.7: The $\Sigma\eta_{\mu,\text{seg}} - \Delta\phi_{\mu,\text{seg}}$ distribution of signal quality muons in VR-μ. The red line and shadow shows the bounds of the full cosmic tag, while the blue line and shadow shows the boundary of the narrow cosmic tag. Everything inside the respective boxes is tagged as a cosmic. The intermediate tag defines the region included in the full tag, but not included in the narrow tag.

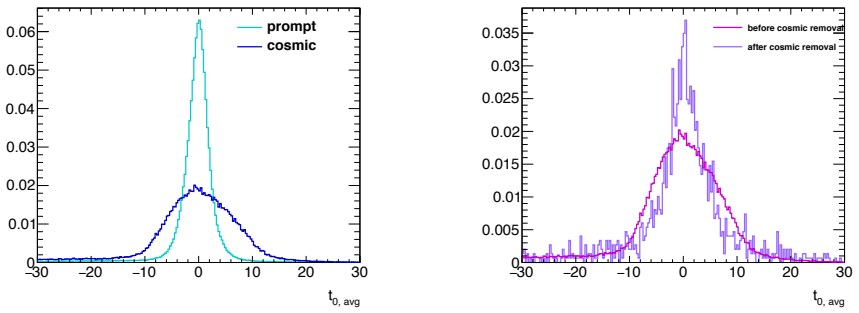

Figure 9.8: t_0^{avg} of cosmic and prompt muons used as templates to the fit (left) and VR-μ dataset before and after removal of cosmic tagged muons on which the fit was performed.

two on either side of the detector, indicating muons from a cosmic shower. In CR-M_{full} events, some jets are seen from pileup collisions, but no additional leptons are observed in events with with cosmic muons. Interesting LHC collisions are rare and so are cosmic muons, so the odds of having the two coincident in the same bunch crossing is minuscule. Generally, the cosmic muon is the most notable feature of the event and is the reason the event was triggered.

Events with two muons reconstructed from one cosmic muon have a very distinct signature. They have exactly correlated z_0, exactly anti-correlated d_0, equal and opposite ϕ measurement, and their η measurements sum to 0. This can be seen in Figure 9.10.

[Question: talk about the brems rabbit hole? maybe no]

The timing distributions as measured by the MDT segments of muons in 1 and 2 cosmic tagged events can be seen in Figure 9.11. In the 1 μ case, μ_{b} has a timing distribution centered around 0, indicating that μ_{b} is responsible for the trigger decision in these events. However, in 1-μ events in which only μ_{t} passes baseline selections, its timing distribution is shifted negative (early w.r.t the collision), mirroring the distribution for μ_{t} in 2-μ events. This indicates that, even in cases in which only μ_{t} is reconstructed, the trigger decision is made based on μ_{b}.

It takes roughly the same time for a cosmic muon to cross the width of the detector as is the bunch spacing (about 25 ns). This means that in order to have sufficient detector information to reconstruct two muons, the two MS signatures must be at the edges of the

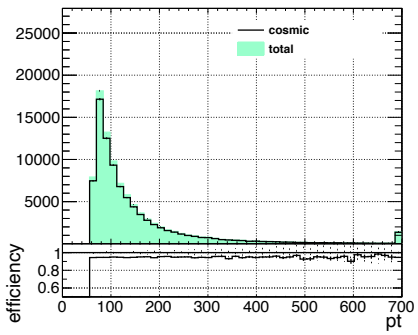

(a) VR-μ data with respect to p_{T}

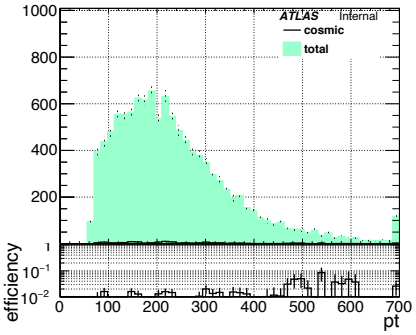

(b) Signal MC with respect to p_{T}

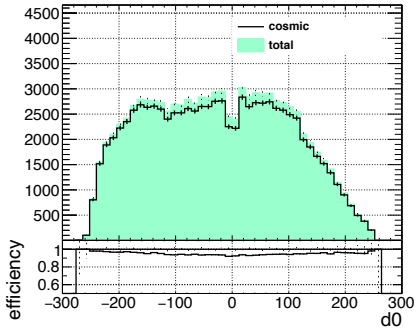

(c) VR-μ data with respect to d_0

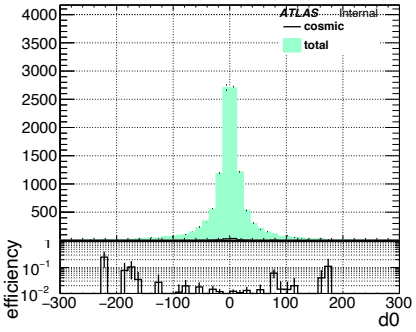

(d) Signal MC with respect to d_0

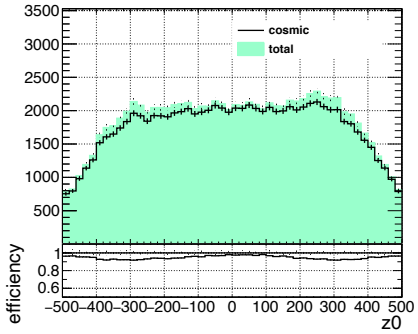

(e) VR-μ data with respect to z_0

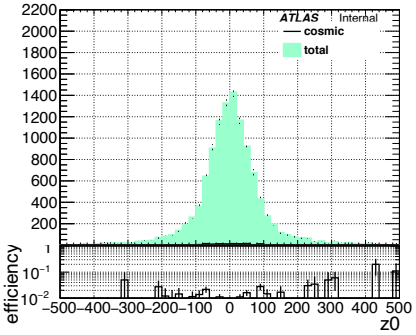

(f) Signal MC with respect to z_0

detector readout window and near the bounds of the t_0^{avg} cut. This makes one or both muons likely to have detector information associated to the wrong event. Due to the early timing of μ_{t}, this is more likely for μ_{t}, but occurs for both μ_{t} and μ_{b}.

Each of the combined muons will pass signal selections, because high quality information exists from the ID, but if enough MS information is missing, the MS segments will not be found back to back with the opposite combined muon, causing one or both of the muons to evade the cosmic tag. Ultimately, it is this mismeasurement that leads to the background in

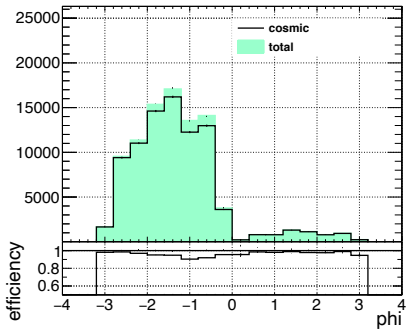

(g) VR-μ data with respect to ϕ

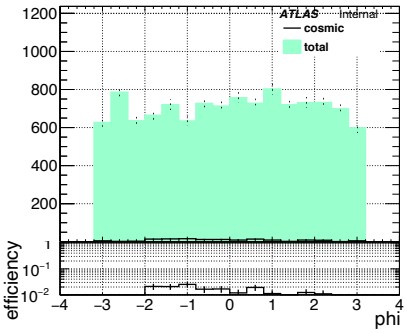

(h) Signal MC with respect to ϕ

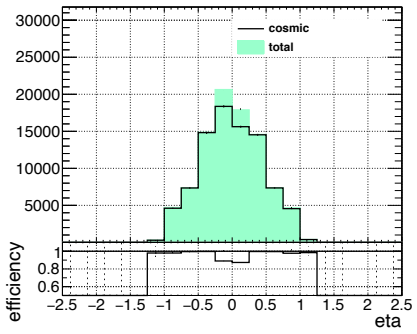

(i) VR-μ data with respect to η

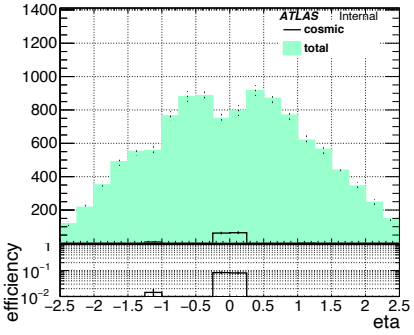

(j) Signal MC with respect to η

Figure 9.9: Cosmic tagging efficiency with respect to kinematic variables in VR-μ data and signal MC

SR-$\mu\mu$.

9.3.3 Background Estimate

If a MS segment is reconstructed without direct ϕ measurements from RPC or TGC hits, its ϕ measurement is taken as the center of the MDT, which has resolution of $\Delta\phi = 0.2$ (the final nominal tag value of $\Delta\phi_{\cos} = 0.25$ was expanded to include these cases). Events with this measurement scheme were seen in a preliminary definition of the cosmic tag, which used the same $\Sigma\eta$ cut, but the $\Delta\phi_{\cos}$ cut was reduced to $\Delta\phi_{\cos} = 0.18$. With this preliminary version of the cosmic tag, about 40 events were observed with one cosmic tagged muon, and another untagged muon. In these events, μ_{t} was missing direct MS ϕ measurements, so its segments were not back-to-back with μ_{b} and μ_{b} was not tagged as a cosmic. μ_{b} however, was well measured, so μ_{t} was cosmic tagged. An event can enter the signal region if both μ_{b} and

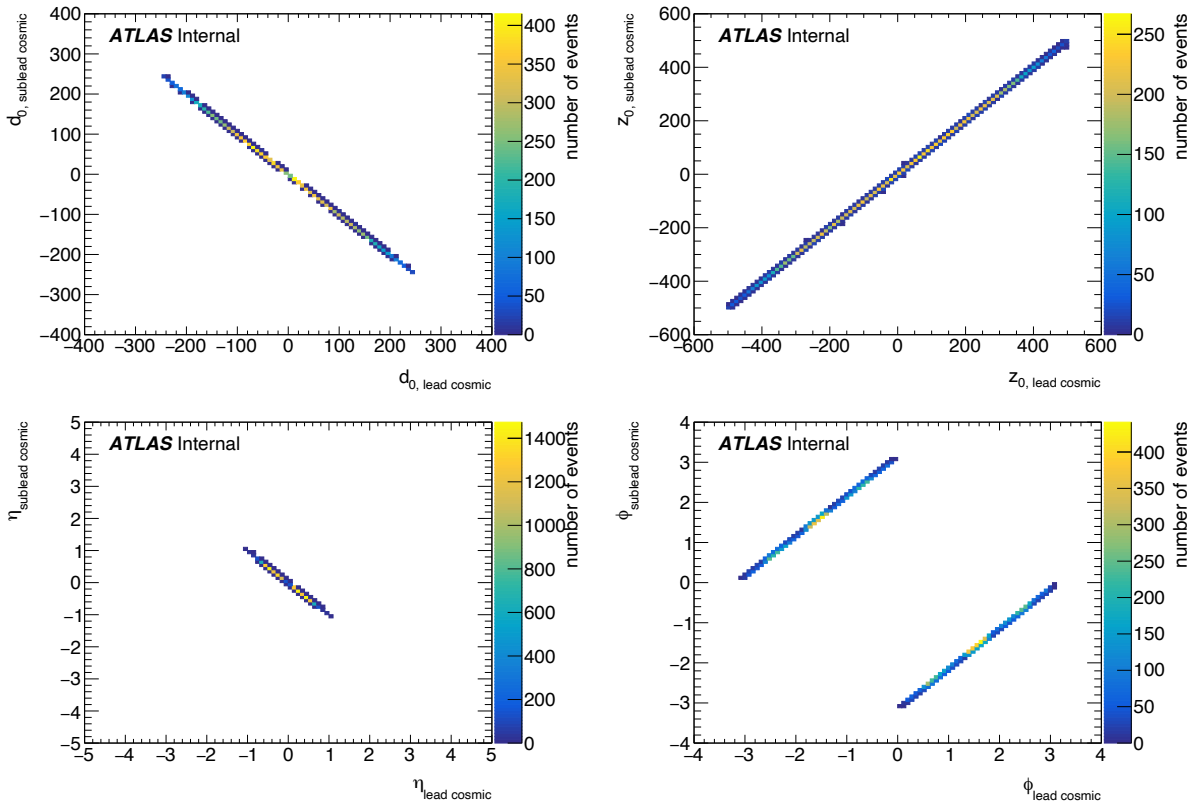

Figure 9.10: Relationship between two cosmic tagged muons in an event. Their d_0 (top left), z_0 (top right), η (bottom left), and ϕ (bottom right) values all indicate that the two muons originate from the same cosmic.

μ_{t} are sufficiently mis-measured that neither can be tagged. This is sketched in Figure 9.12. A muon's cosmic tag is dependent on the opposite muon's quality, so the muon's cosmic tag status and its quality are assumed to be uncorrelated in order to make an estimate of the background.

This estimate and validation makes use of the two cosmic tags described in Table 9.3, as well as an *intermediate tag* which defines a muon that is not tagged by the narrow tag but is tagged by the nominal tag. Because a cosmic muon is defined using detector information on the opposite side of the detector, muons tagged using the narrow tag must have a higher quality measurement on the opposite side of the detector in order to pass the tighter cuts than those tagged with only the nominal tag. Cosmic tagged muons with $\Delta\phi_{\text{cos}} - \Sigma\eta$ values closer to the edge of the nominal cosmic tag window are more similar to those that would

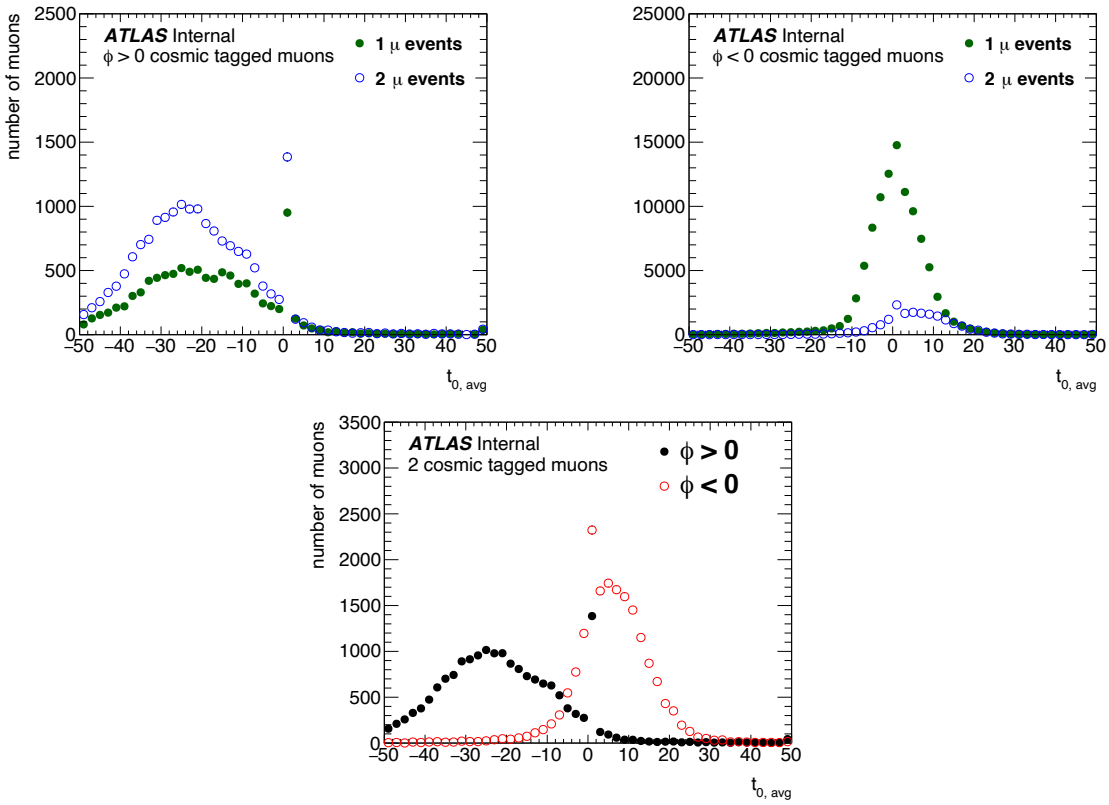

Figure 9.11: Comparison of timing distributions of positive ϕ (top left) and negative ϕ (top right) muons in 1 and 2 cosmic events, as well as the timing distribution of top and bottom muons in 2 cosmic events (bottom). Here, "2 cosmic tagged muons" implies 2 muons reconstructed from 1 cosmic muon. t_0^{avg} is calculated by taking the average of the t_0 measured by all segments associated to the muon. Note that the peak at $t_0^{\text{avg}} = 0$ indicates a failure of the fit used to measure t_0^{avg}, these are handled separately and individual segments with $t_0^{\text{avg}} = 0$ do not enter the t_0^{avg} calculation.

enter SR-$\mu\mu$ as background (which are outside of the cosmic tag window).

To estimate the number of events entering SR-$\mu\mu$ from poorly measured cosmic muon events, a scaling factor from good quality to bad quality muons, R_{good}, is defined. Then, it is used to scale events which have one good quality and one bad quality muon, CR-$\mu\mu$-topbad, into SR-$\mu\mu$ to esimate the background contribution. This is in Figure 9.13. "Good" quality defines a muon that passes signal cuts on N_{prec}, N_ϕ, and χ^2_{CB}, while a "bad" quality muon fails at least one of these cuts. For the nominal version of the estimate, it is assumed that there is one $\phi > 0$ muon (μ_{t}) and one $\phi < 0$ muon (μ_{b}), and μ_{t} is the muon is scaled from "bad" to "good" quality. All regions have 2 reconstructed muons, and the cosmic tag and

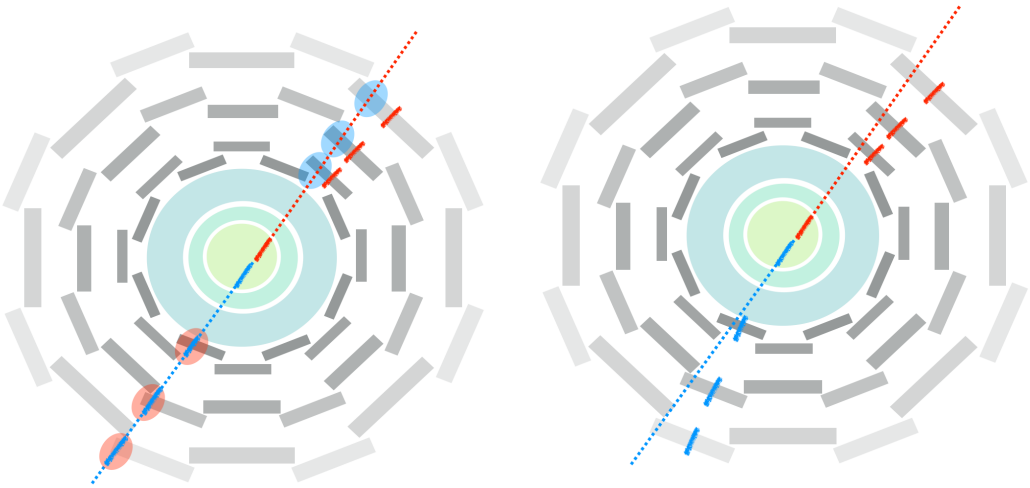

Figure 9.12: Sketches illustrating how a a 2 μ cosmic event could evade a cosmic tag. In this diagram, the thick lines represent ID tracks and MS segments, and the dashed line the CB muon measurement. A muon is tagged as cosmic if it is back to back with an MS segment. If an MS segment does not have a direct ϕ measurement from an RPC hit, its ϕ measurement is taken as the center of the MDT, which has an uncertainty of 0.2 (though the muon can be mismeasured in other ways as well, for example lacking MDT hits or resulting from a bad combination of ID track and MS track). The sketch on the left shows a 2 μ event where the red muon is cosmic tagged but the blue is not. The segments attached to the red muon are not measured well, so when we look for the red segments back to back with the blue muon (the blue circles), the segments are not in the right place and the blue muon is not cosmic tagged. However, the blue muon is well measured, so when we look back to back with the red muon, we find the segments of the blue muon. Thus, the better quality muon is not tagged, while the poorer quality muon is. The right shows a scenario where both muons have this mismeasurement, and so neither is cosmic tagged. This is what contributes to the background in SR-$\mu\mu$.

quality are varied to define the various regions used to make the estimate.

R_{good} for the SR-$\mu\mu$ estimate is defined using muons tagged with the full cosmic tag. A validation estimate is also defined, using the narrow and intermediate cosmic tags. The signal and validation regions used in this estimate are sketched in Figure 9.14 and the numbers of events in each region listed in Table 9.5. Aside from Region 2 (CR-$\mu\mu$-topbad), all other regions in the SR and VR estimates are subsets of CR-M_{full}. These regions were chosen to maintain orthogonality, while minimizing signal contamination and maximizing statistical power. In all cases, statistical errors on R_{good} are computed using the Wilson interval which is recommended for values close to zero with small statistics [34].

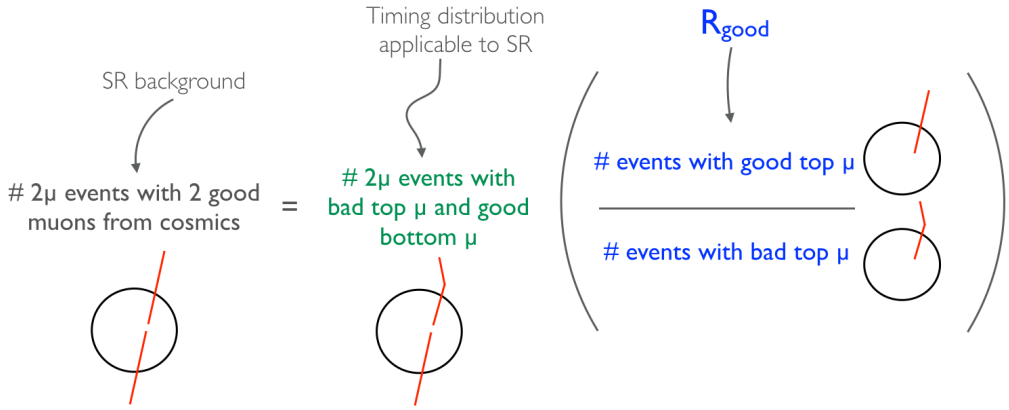

Figure 9.13: A visual representation of the background estimation strategy

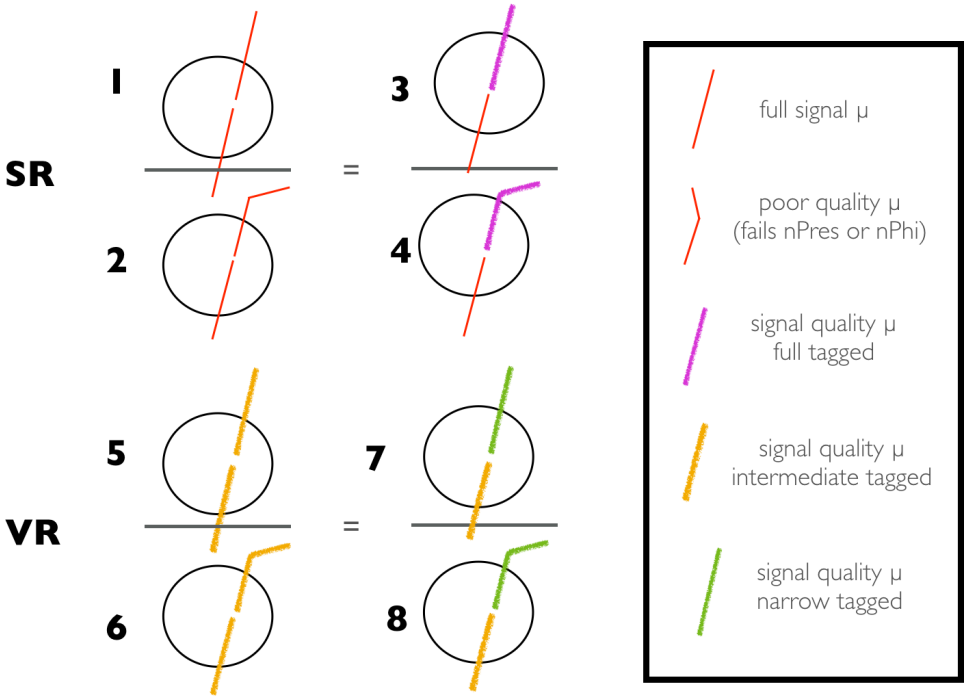

Figure 9.14: A visual representation of the CRs and VRs used to estimate and validate the background contribution to SR-$\mu\mu$ due to cosmic muons. Regions 3 and 4 are used to define R_{good}. These regions were chosen to maintain orthogonality, while minimizing signal contamination and maximizing statistical power.

Results of the estimate and validation are shown in Table 9.6. There is a statistically significant discrepancy between the estimated and actual number of events in the VR. This nonclosure can be explained by the difference in $|d_0|$ distributions in Region 5 and Region 6, shown in Figure 9.15. The excess of low $|d_0|$, high χ^2_{CB} muons in the weighted Region 6

Region	$\phi < 0$ muon	$\phi > 0$ muon
1	signal	signal
2	signal	fails at least one MS quality cut
3	signal	cosmic tagged
4	signal	cosmic tagged and fails at least one quality cut
5	narrow cosmic tagged	narrow cosmic tagged
6	narrow cosmic tagged	narrow cosmic tagged and fails at least one quality cut
7	narrow cosmic tagged	full, but not narrow, tagged
8	narrow cosmic tagged	full, but not narrow, tagged and fails at least one quality cut

Table 9.4: A description of the regions used for the cosmic estimate and validation. Each column describes the way in which the muon deviates from a signal muon, meaning a muon is signal in all respects except for the parameter(s) listed in the table.

Region	1	2	3	4	5	6	7	8
Event Yield	–	2	1	18	1088	1000	1947	2465

Table 9.5: Numbers of events in each region used for the cosmic estimate. Regions 2-4 are used to estimate SR-$\mu\mu$ (Region 1) and Region 6-8 estimate the number of events in Region 5, show in Figure 9.14.

compared to Region 5 implies that more muons have been created due to a poor combination of prompt track with MS track. The estimate was performed in the VR with R_{good} defined as a function of $|d_0|$ and the nonclosure was reduced from 37.7% to 11.7%. It is not possible to perform this estimate as a function of $|d_0|$ in the SR due to low statistics in Region 2 and Region 3. The estimate is performed without the $|d_0|$ binning and the nonclosure from the unbinned estimate in the VR is taken as an uncertainty (37%). In the SR, seen in Figure 9.17, there are no overlapping $|d_0|$ bins in CR-$\mu\mu$-topbad and R_{good}, however, adjacent bins are filled, so the extrapolation over $|d_0|$ is not large and uncertainity from this extrapolation is contained in the nonclosure systematic. R_{good} and $|d_0|$ distributions for each estimate is shown in Figure 9.17 and Figure 9.16 for the SR and VR, respectively.

Region	central value	up error	down error	actual value	% diff from actual
VR	789.9	34.85	34.4	1088	37.7%
SR	0.11	0.20	0.10	–	–

Table 9.6: Results of the background estimation strategy in the two validation regions and the signal region

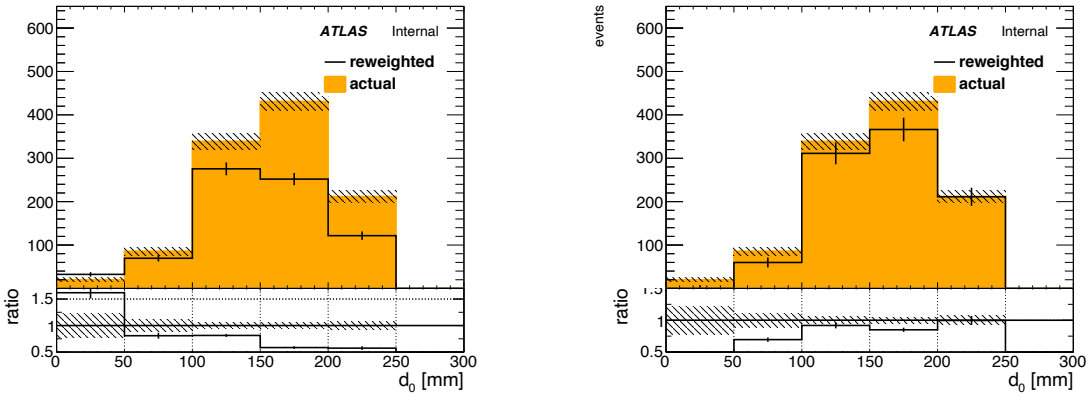

Figure 9.15: Comparison of $|d_0|$ in Region 5 (orange) compared with Region 6 weighted by unbinned $R_{\text{good}} = 0.78$ (left) and by R_{good} defined as a function of $|d_0|$ (right). The nonclosure improves from 37.7% to 11.7% by binning R_{good} in $|d_0|$. The error shown is statistical only. There is no trend in other variables (p_{T}, η, ϕ, z_0, t_0^{avg}).

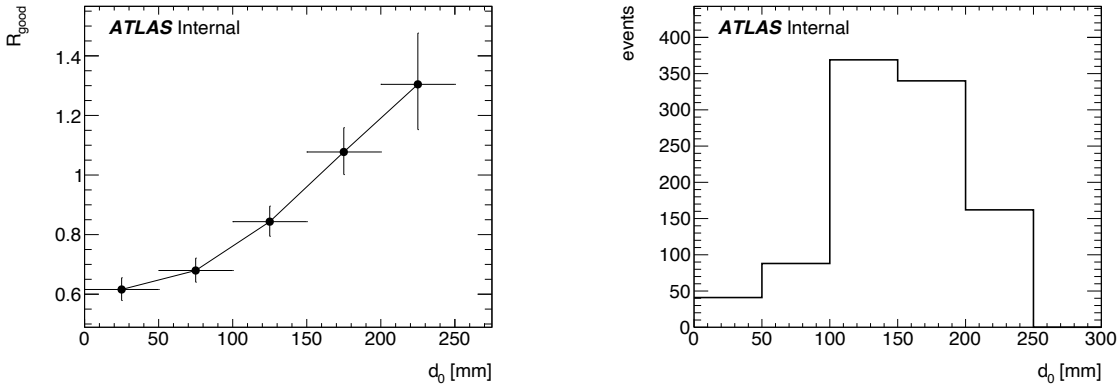

Figure 9.16: $|d_0|$ distribution of R_{good} (left) and μ_{t} in Region 6 to perform the VR estimate. To calculate the background estimate, the distributions are multiplied bin by bin and summed. The error shown is statistical only. This method is ultimately not used, in favor of an unbinned version, due to statistical limitations in the regions used for the SR estimate

9.3.4 Systematic Uncertainties

Muon Orientation The estimate is performed using the quality of μ_{t} since muons in the upper hemisphere are expected to be more temporally marginal and mismeasured. However, the strategy can be performed with the quality of μ_{b}. Because bad quality μ_{b} are more rare bad poor quality μ_{t}, it is not possible to compare this strategy in the SR estimate, which is already statistically limited. However, the comparison can be made in the VR. As shown in Table 9.7, this change produces an estimate that is consistent with the nominal estimate

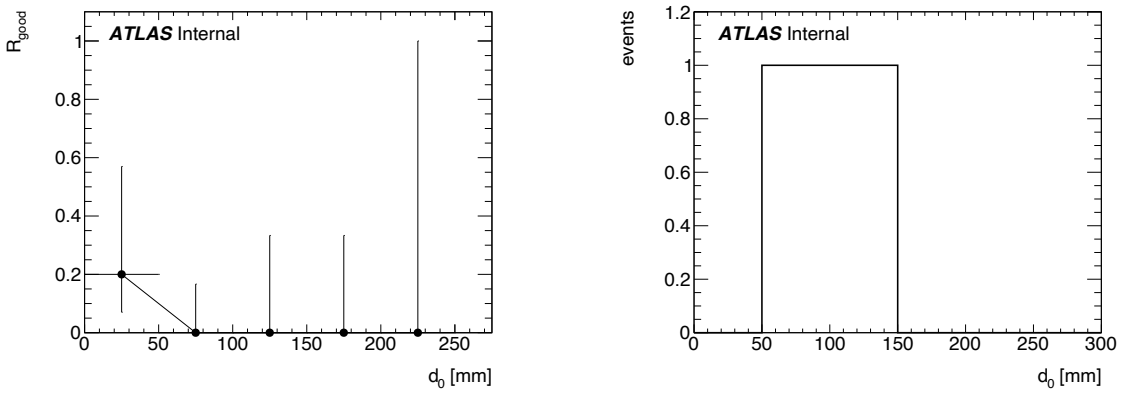

Figure 9.17: $|d_0|$ distribution of R_{good} (left) and μ_{t} in Region 2 to perform the SR estimate. To calculate the background estimate, the distributions are multiplied bin by bin and summed. The error shown is statistical only. It can be seen here that there are no overlapping bins between the two plots, and so this method is ultimately not used, in favor of an unbinned version.

central value	up error	down error	actual value	% diff from actual	% diff from nominal
689.0	115.1	108.8	1088	62.3 %	13%

Table 9.7: Estimate in VR with bottom muon as test muon instead of top muon. CR-$\mu\mu$-topbad becomes VR-$\mu\mu$-bottombad and R_{good} is defined using the quality of μ_{b} instead of μ_{t}.

within statistical uncertainties. Nonetheless, a 13% systematic uncertainty is applied from the difference between the two predictions.

The estimate relies on the assumption that if two muons are reconstructed from a cosmic muon, one will be on the top of the detector and the other on the bottom. 0 events were observed with one good muon and one bad muon on the same side of the detector (sign(ϕ_0) = sign(ϕ_1)) in both the 1 cosmic-tag regions and 0 cosmic-tag regions, so contributions from same-side muons are considered negligible.

Quality parameter dependence In the nominal estimate, a "bad" quality muon means one that fails any one of the N_{prec} or N_ϕ or χ^2_{CB} cuts. To evaluate the dependence one each variable, the estimate can be performed using only one of these to define a "bad" quality muon, requiring the others to pass the signal requirements. However, χ^2_{CB} is dependent on the MS track hit requirements and has a small contribution to the estimate regions on its

Variable	central value	up error	down error	actual value	% diff from actual	% diff from nominal
N_ϕ	783.6	69.2	68.1	1088	38.8%	0.9%
N_{prec}	920.6	51.8	50.9	1088	18.2%	16.5%

Table 9.8: Dependence of the background estimate in the VR on each of the variables used. In each estimate, only the given quality variable is used to define a "bad" muon and the other must always pass. In both cases, the χ^2_{CB} is allowed to pass or fail the signal cut.

Variable	central value	up error	down error	% diff from nominal
N_ϕ	0	–	–	100%
N_{prec}	.33	0.75	0.40	200%

Table 9.9: Dependence of the background estimate in the SR on each of the variables used. In each estimate, only the given quality variable is used to define a "bad" muon and the other must always pass. In both cases, the χ^2_{CB} is allowed to pass or fail the signal cut.

own. Only inverting only χ^2_{CB} leaves 11 events in each Region 6 and Region 8 and 0 in Region 2 and Region 4. Thus, we account for the χ^2_{CB} contribution by remaining agnostic to it in performing the estimate with the other two quality variables. Allowing for the failure of the χ^2_{CB} cut increases the N_{prec}-only and N_ϕ-only estimates by 2% and 1%, respectively. Table 9.8 and Table 9.9 show the results of this procedure in the VR and SR, respectively. We take the largest difference from the nominal estimate in the VR (16.5%) to account for the quality variable dependence.

9.3.5 Summary

This estimate is dominated by statistical uncertainties in the SR estimation regions. Ultimately, $0.11^{+0.20}_{-0.11}$ ($^{+0.198}_{-0.104}$ stat. and 0.047 syst) events are expected in SR-$\mu\mu$ due to cosmic muons.

9.4 Negligible Backgrounds

Since this analysis is built on the assumption that there should be 0 background events in all signal regions, it is extremely important to ensure that all possible backgrounds are accounted for. Three different backgrounds were studied and determined to be negligible,

meaning that they contribute $\mathcal{O}(10^{-4})$ or less events to the relevant SRs.

9.4.1 Material Interactions

Material interactions define events with dilepton pairs that come from interaction with the material of the ATLAS detector. In other searches for long lived particles in ATLAS where displaced vertices (DVs) are required, DVs are reconstructed by extrapolating their tracks to their intersection, and it can be determined if verticies originate from material. In this analysis, there is no vertex so such a veto cannot be used. In order to study material interactions, events with leptons associated to displaced vertices from material were studied. It was found that in the cases of both electrons and muons, events with an DV, where one track is associated to a lepton, the ΔR between the lepton and the other track in the DV was less than 0.2. After making the requirement that $\Delta R_{\ell,\text{track}} < 0.2$, no DVs with signal leptons were found. In the case of the background to one of the SRs, the second track in the DV would be associated to a lepton. After this cut is made, this background is negligible to all 3 SR.

9.4.2 Fake Muons

Fake muons were estimated using an ABCD method similar to SR-ee and SR-$e\mu$. Muons were selected using the baseline requirements, plus asking that be isolated, and not cosmic tagged. All remaining cuts used for defining signal muons were used to define "passing" muons. Using this strategy, only 6 events were seen in the D region, and 0 in either B or C. In the SR-$e\mu$ fake estimate, the ratio of passing to failing muons is less than 1%. Given this, the probability for two fake muons to pass our selections should be less than 0.01%, making this background negligible (< 0.0006 events) and we consider it to be negligible relative to cosmic muons.

Region	SR-ee	SR-$\mu\mu$	SR-$e\mu$
Total background	0.46 ± 0.10	$0.11^{+0.20}_{-0.11}$	$0.007^{+0.019}_{-0.011}$
Fakes + Heavy Flavor	0.46 ± 0.10	$< 10^{-4}$	$0.007^{+0.019}_{-0.011}$
Cosmics	-	$0.11^{+0.20}_{-0.11}$	-

Table 9.10: Summary table of the background estimate and uncertainty in each SR.

9.4.3 Heavy Flavor Muons

Heavy flavor electrons and muons cannot be disentangled from algorithmic fakes in SR-ee and SR-$e\mu$ and are estimated in conjunction with fakes. Fakes are negligible in SR-$\mu\mu$, so a HF estimate must be performed separately. Very few events in $t\bar{t}$ MC have single muons from decays of b-hadrons pass the signal p_{T} and $|d_0|$ cuts, so this background is expected to be small when two muons are required. An ABCD method cannot be used for this estimate because it cannot be assumed that the probability to find an isolated muon is uncorrelated between 2 muons from two HF decays.

First, data was checked for anti-isolated muon events in CR-$\mu\mu$-hf, a region with two signal muons and at least one of the muons must be anti-isolated. No events were observed. Loosening the kinematic cuts to $p_{\mathrm{T}} > 50$ GeV and $|d_0| > 2$ mm also found zero events. Finally, since the muon trigger and thus muon `DRAW_RPVLL` filter only requires one muon, it was possible to study events with one baseline muon and one muon with $|d_0| > 0.5$ mm. One event was observed in this region. Then, extrapolation factors to the SR kinematic cuts were defined from the same dataset. The extrapolation factor from the extremely loosened region into SR-$\mu\mu$ for both the $|d_0|$ and p_{T} of both muons was calculated to be 0.00013 ± 0.00013. This means that 1.3×10^{-4} are expected in SR-$\mu\mu$ from muons from HF, a negligible contribution.

9.5 Summary

In all, < 1 events are expected in each SR. Table 9.10 summarizes the background estimates and Table 9.11 summarizes the systematic uncertainties.

Background	Uncertainty	Value [%]
SR-ee		
Fake and Heavy Flavor	Statistical	18
	HF Nonclosure	11
	Fake Nonclosure	6
	Total	22
SR-$e\mu$		
Fake and Heavy Flavor	Statistical	+260 / -130
	HF Nonclosure	92
	Fake Nonclosure	8
	Total	+270 / -160
SR-$\mu\mu$		
Cosmic Muons	Statistical	+180 / -95
	VR Nonclosure	38
	Estimate variable	16.5
	Muon Orientation	13
	Total	+185 / -104

Table 9.11: Table describing statistical and systematic uncertainties for all background estimates as a percent of total yield. The total uncertainty is the sum of the individual components in quadrature.

CHAPTER 10

SIGNAL SYSTEMATICS

In order to use this analysis to make a statement about a potential BSM model, the extent to which the signal MC correctly simulates the real physical environment must be evaluated. Differences between data and MC are studied in order to avoid underestimating or overestimating the expected number of BSM events that could have been seen in the data.

Where possible, the MC is corrected to better represent the data using *scale factors*, and in other cases systematic uncertainties are applied to the final result. Uncertainties are also evaluated on the scale factors. A list of all of the systematic uncertainties applied in the interpretation are listed in Table 10.1. The value listed in the table describes how much varying the efficiency of a given parameter changes the final signal yield.

The dominant source of systematic uncertainty on the signal MC in this analysis comes from the efficiency for selecting displaced leptons, for which there is no data to compare to MC. As a result, this is evaluated in several steps: first the trigger, reconstruction, and selection efficiencies are compared for prompt leptons in the same physics process in data and MC; then the tracking efficiency is compared between signal muons and cosmic muons, which compares different physical phenomena that result in p_{T}, high $|d_0|$ tracks; finally, the lepton reconstruction efficiency is studied with respect to displacement is studied in MC only and a conservative additional uncertainty to account for any missed effects in data is measured. Other event-level systematic uncertainties are applied to account for mismodeling of pileup and theory assumptions made during MC generation. There are many standard systematic uncertainties derived by ATLAS, for example the jet energy measurements or the sagitta measurements of muons, that do not have a large impact on this analysis with its nonstandard physics objects.

[TODO: update table]

Uncertainty Source	Uncertainty [%] ($\tilde{e}/\tilde{\mu}$)	Uncertainty [%] ($\tilde{\tau}$)
Statistical	2-46	2-100
Cross Section	2-5	2-5
Tracking	2-15	11-14
Muon Trigger	1-4	4
Muon Selection	3-15	20-37
Electron Selection	0.5-2	1-2
Electron Trigger	0	0
Lepton Displacement	1-18	2-26
Pileup Modeling	7	7
Other theory	0-5	0-5
`DRAW_RPVLL` Filter Efficiency	1.5	1.5
Luminosity	2	2

Table 10.1: Table describing statistical and systematic uncertainties impacting $\tilde{e}$, $\tilde{\mu}$ and $\tilde{\tau}$ efficiencies. Systematics in this table are defined as the difference varying each parameter makes in the final signal yield.

10.1 Displaced Lepton Reconstruction

10.1.1 Prompt Lepton Reconstruction

Z bosons can decay into two electrons or two muons. This process is well modeled in MC, and easy to identify in data as the invariant mass of the two leptons should equal the Z boson mass (within resolution effects). The invariant mass of the leptons provides a way to identify a lepton as a real lepton that should pass all of the trigger, reconstruction, identification, and selection algorithms. A *tag-and-probe* analysis *tags* events by finding two lepton candidates with invariant mass near the Z boson peak, and then the *probe* leptons are used to measure the selection efficiency by asking that one of the leptons pass a given requirement. This method is used to evaluate trigger, reconstruction, and selection efficiencies of prompt electrons and muons.

The difference between data and MC can be thoroughly studied, so scale factors are applied to correct the leptons in MC. A scale factor is defined as:

$$\text{scale factor} = \frac{\text{efficiency in data}}{\text{efficiency in MC}} \tag{10.1}$$

Then the statistical uncertainty on this value is evaluated and applied as an additional uncertainty on the signal. In general, MC estimates higher efficiencies than are seen in data. In particular, the MC assumes a perfectly aligned detector with all subsystems working perfectly, which is not true in practice, so variables that correlate multiple subdetectors, like electron $\Delta p_{\mathrm{T}}/p_{\mathrm{T}}$ or muon χ^2_{CB}, contribute to a difference between data and MC. A 90% scale factor means that MC overestimates the selection efficiency by 10%.

ATLAS centrally defines electron and muon scale factors for prompt electrons and muons, but due to the special triggers and selection criteria used in this analysis, custom scale factors are required. For electrons, this analysis uses photon triggers as well as a bug-fixed electron reconstruction, as well as a custom identification and non-standard selection criteria, so all scale factors must be derived specifically for this analysis. For muons, a nonstandard trigger is used, but the reconstruction is standard (except for the tracking, evaluated separately) and the only change to the identification criteria is the removal of the cut on pixel hits, which does not impact prompt muons, so central scale factors are used, with additional selection and special trigger scale factors derived for this analysis.

[Question: I never talked about the electron bug.. i assume that's fine?]

Electrons

For electrons, $Z \to ee$ events are used to evaluate trigger scale factors, and a single scale factor for reconstruction, identification, and selection as all electrons coming from the Z are real electrons and should pass the trigger as well as all selection criteria.

For both `HLT_2g50_loose` and `HLT_g140_loose` triggers, the efficiency is defined as the number of electrons passing the trigger divided by the number of electrons passing the offline identification criteria. This is done for single electrons, and in the case of the 2 electron trigger, the results are summed in quadrature. It was found that above the trigger threshold, the trigger efficiency in both data and MC is very close to 100%, so this scale factor and its associated uncertainty is considered negligible.

The reconstruction, identification, and selection scale factors are evaluated together, by measuring the efficiency for a reconstructed electron candidate to pass the final signal selection. Electron candidates are cluster-track combinations that will get eventually identified as a photon, converted photon, or electron (or none of these). The track reconstruction is studied separately and the cluster reconstruction efficiency at the signal p_{T} is nearly 100%. The scale factors for electron selection are defined as a function of E_T and η and around 98% except for in the region between the barrel and endcap (around $|\eta| = 1.5$) where it drops to 90%. The statistical uncertainty varies from 1-3%.

Muons

$Z \to \mu\mu$ data and MC are used to define additional scale factors for the `HLT_mu60_0eta105_msonly` trigger. The standard trigger scale factors correct for many features of the MS and additional corrections are derived and applied on top of them for this analysis. Events are required to pass a Missing Transverse Energy (MET) trigger to ensure an unbiased data sample and have two muons within 10 GeV of the mass of the Z boson. The trigger efficiency is then defined as the number of muons passing the `HLT_mu60_0eta105_msonly` trigger divided by the number of baseline muons. Similarly, selection scale factors are defined by requiring that one muon pass all signal selections (except the $|d_0|$ cut), then the efficiency for the second baseline muon to pass the same signal selection cuts is evaluated.

The scale factors are larger for muons than for electrons because many of the structural features of the MS are not well modeled in MC. The statistical errors are also around 3%.

10.1.2 Tracking

This analysis relies on LRT in order to reconstruct leptons with high p_{T} and high $|d_0|$. Tracks from cosmic muons have high p_{T} and high $|d_0|$ and can be used to measure the tracking efficiency in data. Cosmic muons are tagged as muons with MS activity on the other side of the detector, so the cosmic muon must have also passed through the ID leaving

a track behind. Provided we make some kinematic selections, the existence of the track back-to-back with the cosmic should be solely dependent on the LRT efficiency.

A tag-and-probe analysis is performed here as well, by tagging a cosmic muon and looking for tracks back-to-back with it in a narrow $\Delta R_{\cos}$ cone. Then compare this to a tag-and-probe analysis in signal MC by looking for a track in a narrow ΔR cone nearby a truth muon.

There are several important kinematic selections that must be made to ensure the collection of tracks are similar and to correct for the different kinematic distributions between cosmics and data (see Figure 9.9).

First, to ensure all the hits in the track will be read out with the event, $\phi > 0$ muons must have negative t_0^{avg} (early w.r.t collision), and $\phi < 0$ muons must have positive t_0^{avg} (late w.r.t collision). Making this cut shows a flat reconstruction efficiency w.r.t. t_0^{avg}. All signal muons have very central timing, with ID signatures created before MS signatures, so this problem does not apply. The impact of the timing cut can be seen in Figure 10.1.

Second, the cosmic ray muon passes through the detector in an approximately straight line through the ID, so the d_0 is simply the distance the cosmic muon was from the PV. This is not the case for signal muons, whose d_0 does not measure a point the muon has gone through, but an extrapolation backwards to the PV. This means that signal tracks with the same d_0 can have very different properties, such as number of hits on track. To correct for this, we require the R_{decay} and d_0 to fall between the same two silicon layers. A sketch of this difference can be seen in Figure 10.2.

Finally, cosmic muons have a much wider z_0 range than signal muons, which induces an η dependence. So we require cosmic muons to have $|z_0| < 120$ mm, to harmonize with signal muons. Additionally, both signal and cosmic muons must have $|\eta| < 1.05$ in order to be triggered. A full list of cuts made on tag muons and probe tracks can be found in Table 10.2 and Table 10.3.

The remaining difference between cosmic and signal muons is the correlation between

p_{T} and $|d_0|$ in signal. Thus, the cosmic muon p_{T} distribution is reweighted in each $|d_0|$ bin to match the signal distribution. Then, the ratio of the efficiencies as a function of $|d_0|$ is determined per lepton. The maximum difference, 8%, is taken as the systematic uncertainty per lepton, then summed in quadrature for the two leptons in the event resulting an 11% event-level systematic. Tracking efficiency is assumed to be symmetric around the detector and that after GSF tracking, electron tracking and muon tracking have equivalent efficiency, motivated by Figure 10.3.

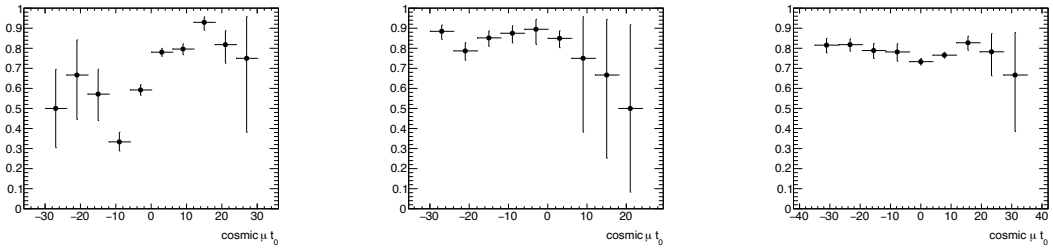

Figure 10.1: LRT efficiency measured with various ϕ and t_0^{avg} cuts. The right shows $\phi < 0$ muons with no t_0^{avg} cut, the center shows $\phi > 0$ muons with no t_0^{avg} cut, and the left shows the final selections, with $\phi > 0$ requried to have t_0^{avg} ¡ 0 and $\phi < 0$ t_0^{avg} ¿ 0. This gives a consistent readout configuration and an approximately flat efficiency w.r.t t_0^{avg}. In particular, there $\phi < 0$ muons with negative timing that result in an artificially low efficiency, likely due to incomplete readout.

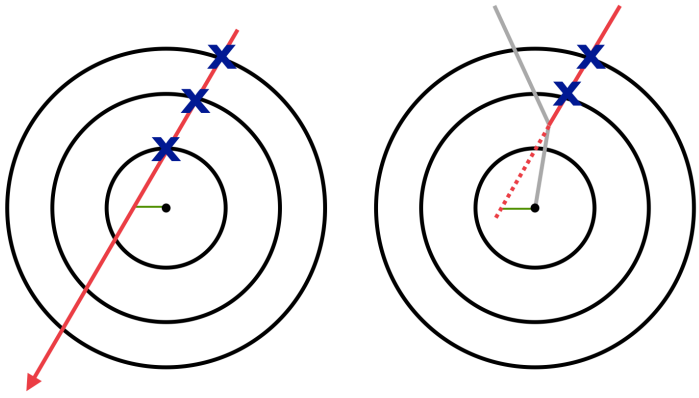

Figure 10.2: An illustration of the difference in d_0 measurements between cosmic (left) and signal muons. The d_0 of a cosmic muon is always measured just before its first hit, whereas for a signal muon, the first hit can come far after the d_0. The blue x's represent ID hits and the red lines represent muon tracks.

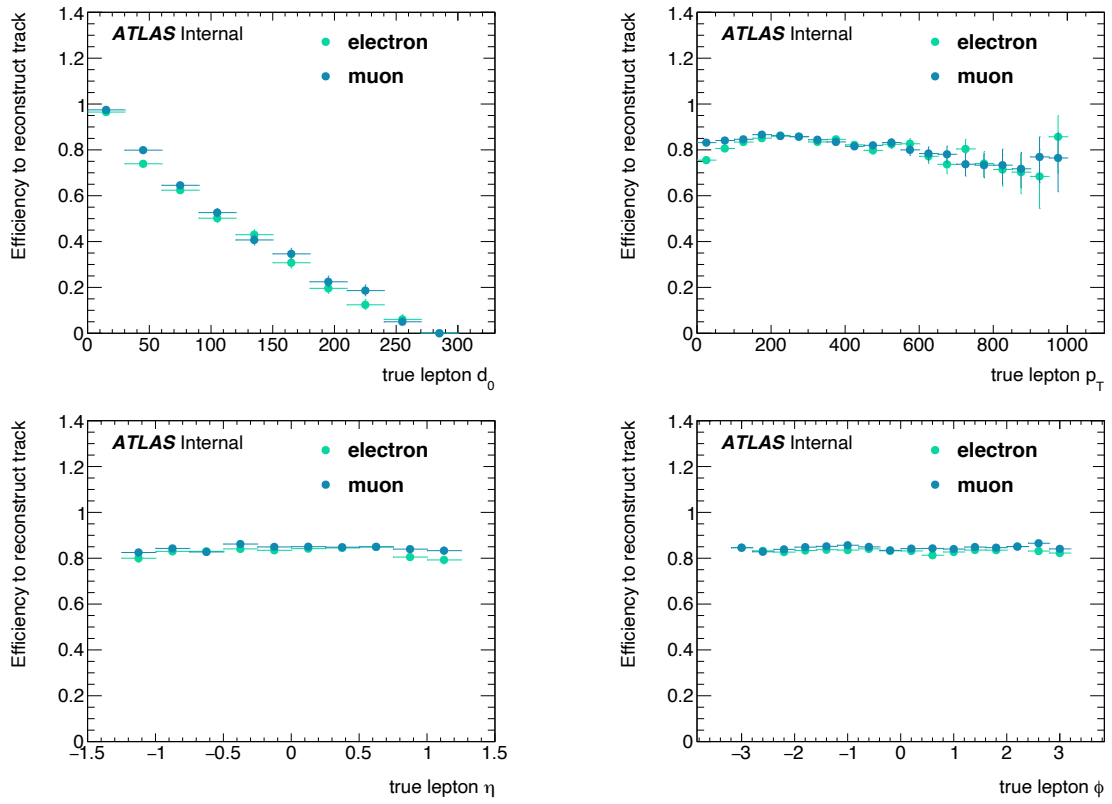

Figure 10.3: Tracking efficency for electrons and muons in signal MC (all lifetimes of 300 GeV $\tilde{e}$ or $\tilde{\mu}$). These plots justify the assumption that tracking efficiency is the same between electrons and muons and symmetric about the ID volume.

Cut on cosmic muon	Cut on truth muon
$p_{\mathrm{T}} > 50$ GeV	$p_{\mathrm{T}} > 50$ GeV
$\lvert d_0 \rvert > 3$mm	$\lvert d_0 \rvert > 3$mm
$\lvert \eta \rvert < 1.05$	$\lvert \eta \rvert < 1.05$
$\lvert z_0 \rvert < 120$ mm	parent is a $\tilde{\mu}$
$t_0^{\mathrm{avg}} > 0$ if $\phi_\mu < 0$ OR $t_0^{\mathrm{avg}} > 0$ if $\phi_\mu > 0$	d_0 and R_{decay} between the same silicon layers

Table 10.2: Cuts on tag muons. Cosmic muons (right) and truth signal muons (left).

Cut on cosmic muon	Cut on truth muon
$p_{\mathrm{T}} > 30$ GeV	$p_{\mathrm{T}} > 30$ GeV
$\Delta R_{\cos} = \sqrt{(\Delta\phi - \pi)^2 + (\Sigma\eta)^2} < 0.3$	$\Delta R = \sqrt{(\Delta\phi)^2 + (\Delta\eta)^2} < 0.05$
$\lvert d_{0,\mathrm{track}} - d_{0,\mu} \rvert < 20$	
$\lvert z_{0,\mathrm{track}} - z_{0,\mu} \rvert < 20$	

Table 10.3: Cuts on probe ID tracks. In data (right) and signal (left).

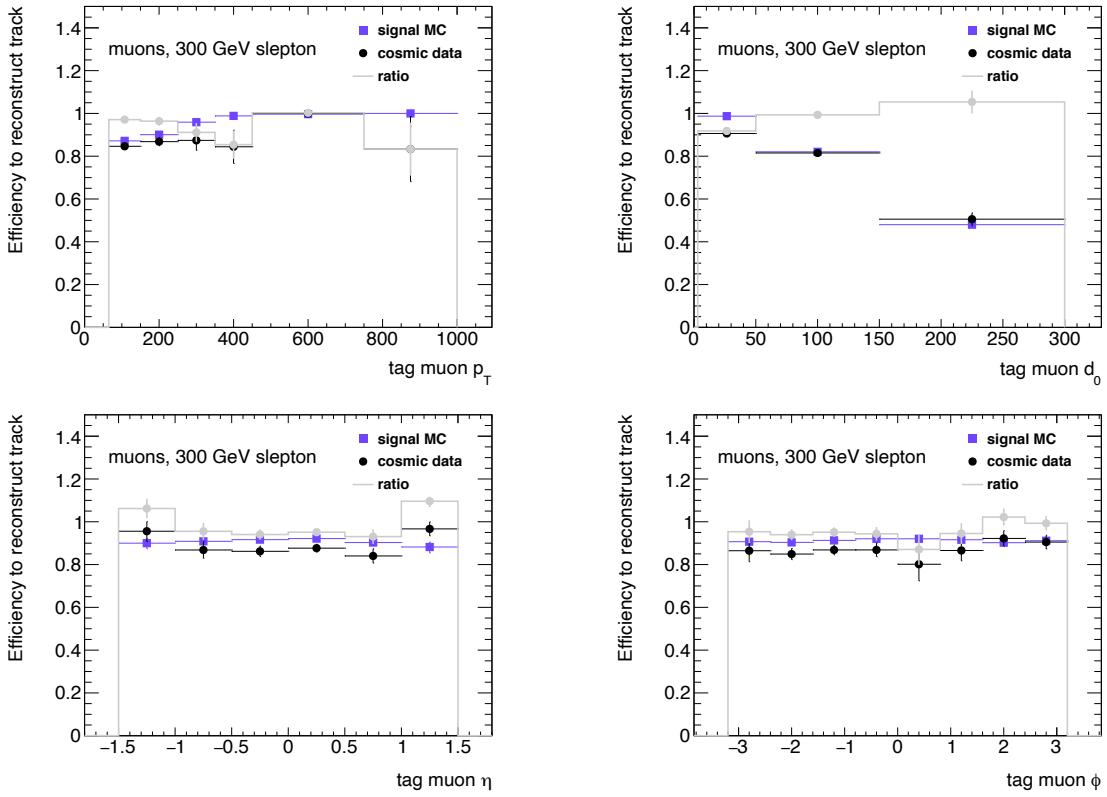

Figure 10.4: A comparison of tracking efficiency in cosmics data and signal MC (all masses and lifetimes can be used to due the eventual p_{T} and d_0 binning) with respect to p_{T} (top left), d_0 (top right), η (bottom left), and ϕ (bottom right). The MC efficiency is shown in purple, the data efficiency in black, and the ratio between the efficienceis is shown in gray.

10.1.3 Lepton Displacement

The effect of displacement on lepton reconstruction cannot be directly compared between data and MC. An additional uncertainty is defined in MC to account for reconstruction effects potentially not captured by the previous two systematic uncertainties. It is taken as the deviation in the reconstruction efficiency as a function of $|d_0|$ relative to prompt muons. This uncertainty is meant to capture any discrepancy in MS track or electron shower shape parameters at high $|d_0|$, as well as changes in how they are combined with the ID track. This uncertainty is extremely conservative as there is no way to determine if the same fluctations are seen in data.

To determine the systematic uncertainty due to displaced reconstruction, the baseline or signal reconstruction/selection efficiency is divided by the tracking efficiency in order to separate any inefficiences from LRT. Then, the ratio of each high d_0 bin relative the prompt bin (0–3 mm) is taken, results of this are shown in Fig. 10.7. The uncertainty is assigned to each lepton and they are summed in quadrature to get an event level systematic.

This uncertainty for muons is quite small, while it is much more substantial for electrons. Electrons are identified using a likelihood, which is trained with d_0 as a discriminating variable. $|d_0|$ was removed from the cuts performed offline, but the LH was not retrained, and so there as a larger relic d_0 dependence and the displacement uncertainty is much larger.

10.1.4 Other Sources of Uncertainty

Pileup Modeling

When MC is generated, particularly when it is generated during the course of the run, the actual pileup distribution of the events from the LHC is not known. This is corrected through a process called *pileup reweighting*, where a more realistic pileup profile is added to MC events. The change in number of signal events when the pileup profile is varied is taken as a systematic uncertainty, 2%.

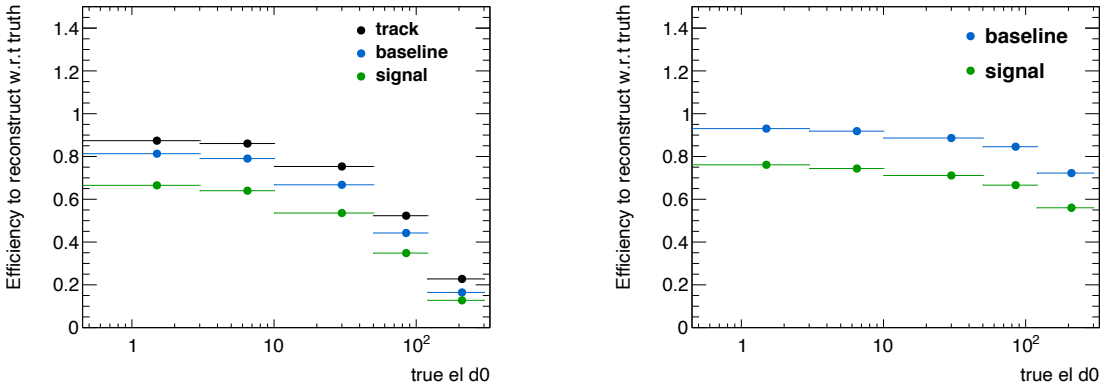

Figure 10.5: Electron selection efficiencies with respect to truth (left) and with respect to the tracking efficiency (right). Made from a 300 GeV $\tilde{\ell}$ signal samples with lifetimes between 0.01 ns-1 ns. The denominator of the efficiency is truth electrons from $\tilde{e}$ with $p_{\mathrm{T}} > 65$ GeV and $|\eta| < 2.5$, and the numerator is truth matched and signal (or baseline) quality tracks or leptons.

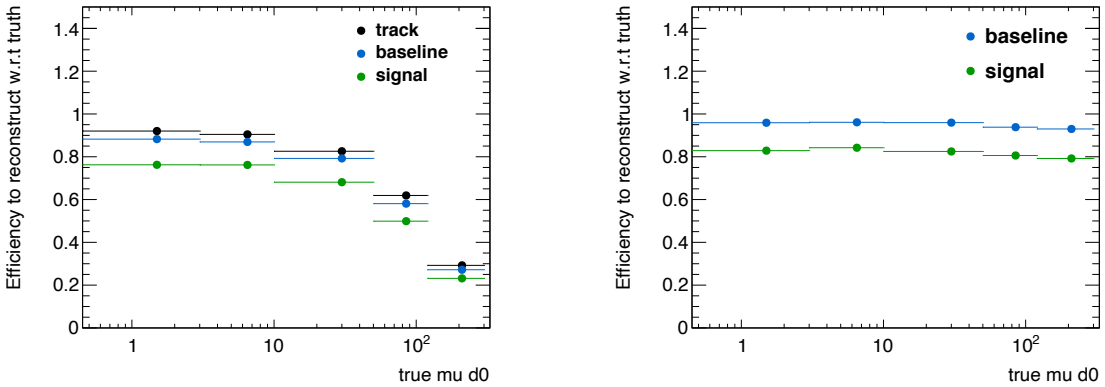

Figure 10.6: Muon selection efficiencies with respect to truth (left) and with respect to the tracking efficiency (right). Made from 300 GeV $\tilde{\ell}$ signal samples with lifetimes between 0.0 1ns-1 ns. The denominator of the efficiency is truth muons from $\tilde{\mu}$ with $p_{\mathrm{T}} > 65$ GeV and $|\eta| < 2.5$, and the numerator is truth matched and signal (or baseline) quality tracks or leptons.

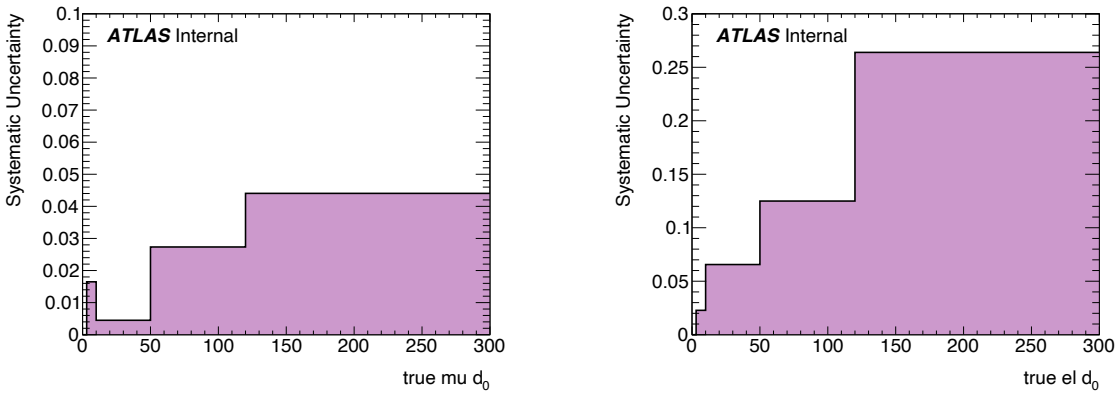

Figure 10.7: Fractional systematic uncertainties defined for muons (left) and electrons. The value of each bin is defined as 1 minus the ratio of the selection efficiency with respect to tracking efficiency of the given bin to the same value of the prompt (0-3 mm) bin. These are defined in 300 GeV $\tilde{\ell}$ signal samples with lifetimes between 0.01 ns-1 ns. It was confirmed that the trends are consistent across various $\tilde{\ell}$ masses.

Theoretical Uncertainties

Additional uncertainties are taken for the renormalization and factorization scales that are used to generate the physical processes in MC. These impact both the cross section measurement and the final lepton kinematics. Both scales are varied, impact on the final results quantified, and the range of variation is taken as an uncertainty, in this analysis about 5%.

Luminosity Measurement

ATLAS measures luminosity using dedicated detectors and calibrations (discussed in section 3.4. The uncertainty on this measurement contributes a 2% uncertainty to the analysis, as it impacts the normalization of the signal yield from MC.

CHAPTER 11

RESULTS

11.1 Signal Yield

0 events are observed in each signal region, in full agreement with the background estimate. The result of each cut made in each SR can be seen in Table 11.2, Table 11.1, and Table 11.3 for SR-$\mu\mu$, SR-ee, and SR-$e\mu$, respectively. The most powerful background discriminators are the $\Delta p_{\mathrm{T}}/p_{\mathrm{T}}$ cut for electrons and cosmic veto for muons, also in agreement with expectations.

This analysis was designed to be as general as possible, so the results can be applied to any new physics signature that results in 2 leptons with high $|d_0|$ and high p_{T}.

Cut	data yield
Pass trigger and at least 2 baseline leptons	65484
2 leading leptons are electrons	19419
$p_{\mathrm{T}} > 65$ GeV	14061
$\lvert d_0 \rvert > 3$ mm	11589
both electrons pass isolation	9220
$\Delta p_{\mathrm{T}}/p_{\mathrm{T}} \geq$ -0.5	7
$\chi^2_{\mathrm{ID}} < 2$	2
$N_{\mathrm{miss}} \leq 1$	0
$\Delta R_{\ell\ell} > 0.2$	0

Table 11.1: Cutflow for SR-ee for Run 2 data.

Cut	data yield
Pass trigger and at least 2 baseline leptons	65484
2 leading leptons are muons	45845
$p_{\mathrm{T}} > 65$ GeV	35607
$\lvert d_0 \rvert > 3$ mm	35326
both muons pass isolation	35204
muons pass cosmic veto	2
$t_0^{\mathrm{avg}} < 30$	2
$\chi^2_{\mathrm{ID}} < 2$	2
$N_{\mathrm{miss}} \leq 1$	2
$N_{\mathrm{prec}} \geq 3$	0
$\chi^2_{\mathrm{CB}} < 3$	0
$N_\phi > 0$	0
$\Delta R_{\ell\ell} > 0.2$	0

Table 11.2: Cutflow for SR-$\mu\mu$ for Run 2 data.

Cut	data yield
Pass trigger and at least 2 baseline leptons	6548
2 leading leptons are a muon and an electron	1910
$p_{\mathrm{T}} > 65$ GeV	128
$\lvert d_0 \rvert > 3$ mm	107
both leptons pass isolation	98
muon pass cosmic veto	86
muon $t_0^{\mathrm{avg}} < 30$	82
muon $\chi^2_{\mathrm{ID}} < 2$	72
muon $N_{\mathrm{miss}} \leq 1$	68
muon $N_{\mathrm{prec}} \geq 3$	6
muon $\chi^2_{\mathrm{CB}} < 3$	0
muon $N_\phi > 0$	0
electron $\Delta p_{\mathrm{T}}/p_{\mathrm{T}} \geq$ -0.5	0
electron $\chi^2_{\mathrm{ID}} < 2$	0
electron $N_{\mathrm{miss}} \leq 1$	0
$\Delta R_{\ell\ell} > 0.2$	0

Table 11.3: Cutflow for SR-$e\mu$ for Run 2 data.

11.2 Interpretation

Since no events are observed, limits are set on the parameter space of GMSB SUSY mdoels. Limits are computed using HistFitter [35], an ATLAS framework that combines the observed number of events with uncertainties on background predictions and signal systematics and calculates both model dependent and model independent limits using the CL_s technique [36]. CL_s is a useful tool for particle physics analyses. Somewhere between a purely frequentist and purlely basian method of deriving a confidence interval, the CL_s describes the confidence in a signal-only hypothesis. The limit curve is drawn where $CL_s(m_{\tilde{\ell}}) \leq 5\%$, meaning that the probability of having falsely excluded a $\tilde{\ell}$ of a given mass is less than or equal to 5%. The smaller the value of CL_s, the lower the probability that a $\tilde{\ell}$ with a given mass exists.

11.2.1 Slepton Limits

Limits are set on the possible masses and lifetimes of long-lived $\tilde{\ell}$. Four different limits are set using the results of this analysis: each $\tilde{e}$, $\tilde{\mu}$, or $\tilde{\tau}$ NLSP, or the mass degenerate case with all three as co-NLSPs. Results for all four scenarios combined are shown in Figure 11.1, and the individual limit for each of the four scenarios along with their observed CL_s value is shown in Figure 11.2.

For the $\tilde{e}$ NLSP and $\tilde{\mu}$ NLSP cases, the results from SR-ee and SR-$\mu\mu$, respectively, are used. While for the $\tilde{\tau}$ and co-NLSP cases, all three SRs are combined. For a lifetime of 0.1 ns, $\tilde{e}$ NLSP, $\tilde{\mu}$ NLSP, $\tilde{\tau}$ NLSP, and co-NLSP scenarios are excluded for $\tilde{\ell}$ masses up to 720 GeV, 680 GeV, 340 GeV, and 820 GeV, respectively. Co-NSLP events are also excluded up to 10 ns for masses below 330 GeV. The previous from OPAL [1] is surpassed by nearly an order of magnitude for $\tilde{e}$-, $\tilde{\mu}$-, and co-NSLP scenarios.

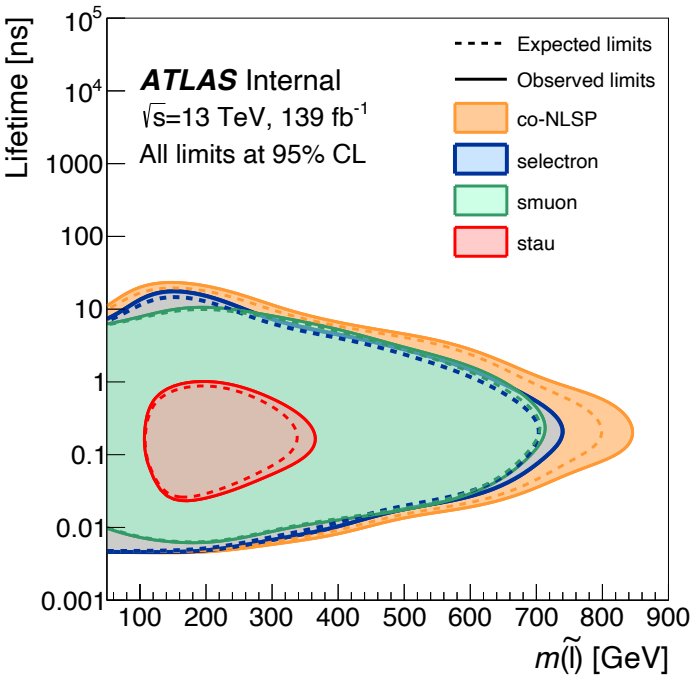

Figure 11.1: Expected (dashed) and observed (solid) exclusion contours for $\tilde{e}$ NLSP, $\tilde{\mu}$ NLSP, $\tilde{\tau}$ NLSP, and co-NLSP production as a function of the lifetime at 95% CL.

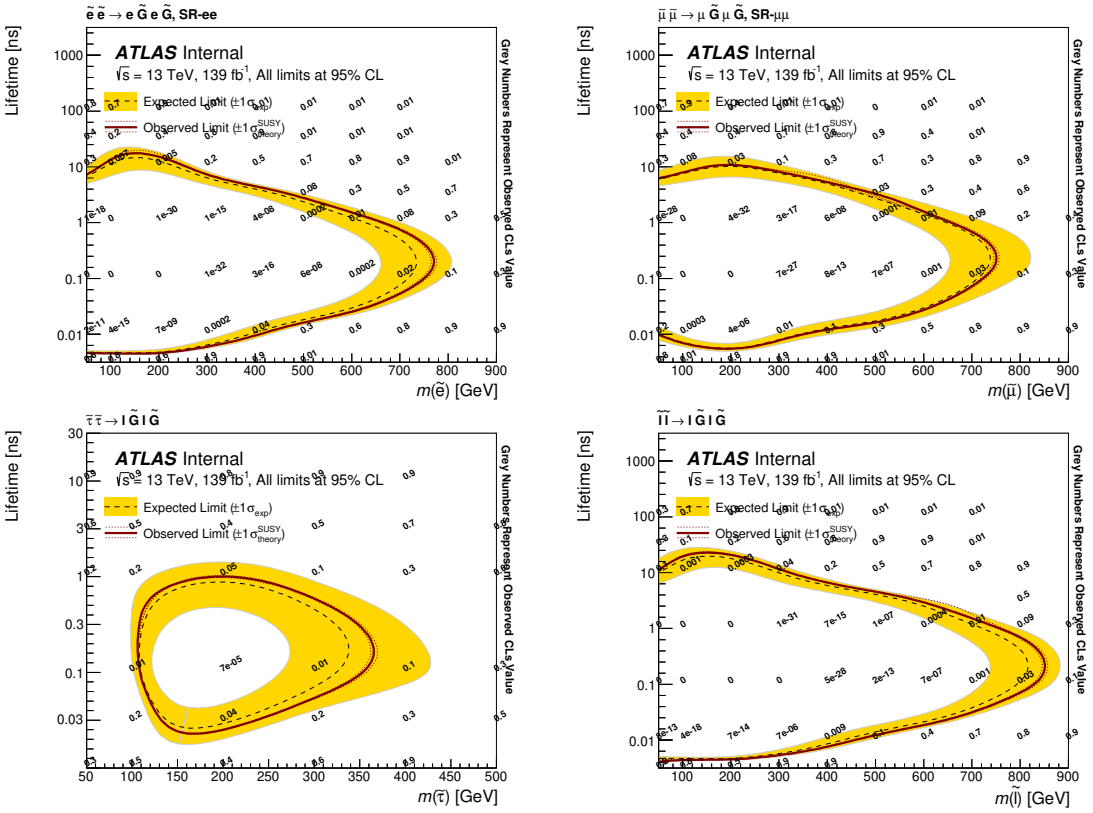

Figure 11.2: Individual exclusion curves for four different NLSP scenarios: $\tilde{e}$ (top left), $\tilde{\mu}$ (top right), $\tilde{\tau}$ (bottom left), co-NLSP (bottom right). Overlaid numbers represent the observed CLs values.

11.2.2 Model-Indpendent Limits

Additionally, model independent limits are set on generic new physics processes in the SRs. These limits are based on the visible cross-section of new physics ($\langle\epsilon\sigma^{95}_{\text{obs}}\rangle$) and the observed ($S^{95}_{\text{obs}}$) and expected ($S^{95}_{\text{exp}}$) number of signal events that would be measured. Visible BSM cross sections above 0.02 fb are excluded in each SR These values are shown in Table 11.4

Signal channel	$\langle\epsilon\sigma\rangle^{95}_{\text{obs}}$[fb]	S^{95}_{obs}	S^{95}_{exp}	$p(s=0)$
SR-ee	0.02	3.0	$3.1^{+1.1}_{-0.1}$	0.47
SR-$\mu\mu$	0.02	3.0	$3.0^{+0.1}_{-0.0}$	0.72
SR-$e\mu$	0.02	2.7	$3.0^{+0.0}_{-0.0}$	0.10

Table 11.4: Left to right: 95% CL upper limits on the visible cross section ($\langle\epsilon\sigma\rangle^{95}_{\text{obs}}$) and on the number of signal events (S^{95}_{obs}). The third column (S^{95}_{exp}) shows the 95% CL upper limit on the number of signal events, given the expected number of background events. The last column shows the p-value of the no-signal hypothesis.